PROVENANCE, STRATIGRAPHIC ARCHITECTURE, AND HYDROGEOLOGIC INFLUENCE OF TURBIDITES ON THE MID-OCEAN RIDGE FLANK OF NORTHWESTERN CASCADIA BASIN, PACIFIC OCEAN

MICHAEL B. UNDERWOOD,[1] KIMBERLEY D. HOKE,[1]* ANDREW T. FISHER,[2] EARL E. DAVIS,[3] EMILY GIAMBALVO,[2]**
LARS ZÜHLSDORFF,[4] AND GLENN A. SPINELLI[2]***

[1] *Department of Geological Sciences, 101 Geology Building, University of Missouri, Columbia, Missouri 65211, U.S.A.*
[2] *Earth Sciences Department, University of California, Santa Cruz, California 95064, U.S.A.*
[3] *Pacific Geosciences Centre, Geological Survey of Canada, Box 6000, Sidney, British Columbia V8L 4B2, Canada*
[4] *Department of Geosciences, P.O. Box 33 04 40, University of Bremen, 28334 Bremen, Germany*
email: UnderwoodM@missouri.edu

ABSTRACT: **The northwestern edge of Cascadia Basin (North Pacific Ocean) is unusual because late Pliocene to Holocene turbidites lap onto juvenile oceanic crust of the Juan de Fuca Ridge. Subsidence of the ridge flank combines with irregular westward progradation of the turbidite facies to create a stratigraphic section that coarsens and thickens upward. The sand provenance is mixed. Individual turbidity currents have funneled into the area through several shelf–slope and abyssal-floor conduits, including Vancouver Valley, Juan de Fuca Channel, Barkley Canyon, and Nitinat Canyon. Local bathymetric blockage, deflection and reflection of flow paths by basement relief, remobilization by intrabasinal submarine slides and debris flows, episodic channel switching, and sporadic overbank flooding have combined to produce erratic recurrence intervals for the turbidity currents. Only the tallest basement highs have remained isolated from turbidite deposition during the last 500,000 years. Spatial and temporal differences in sediment accumulation are important because they modulate the three-dimensional responses of compaction and consolidation. Those changes in physical properties govern where and when hydraulic communication with the underlying basement shuts down. The basal hemipelagic layer of Cascadia Basin transforms to an effective hydrologic seal (seepage rates < 1 mm/yr) once the sediment–basalt interface is buried by 100–150 m of strata. Rapid accumulation of turbidites, therefore, accelerates the hydrogeologic conversion of igneous basement from open to sealed.**

INTRODUCTION

Cascadia Basin is located in the northeast Pacific Ocean off the coastline of northernmost California, Oregon, Washington, and British Columbia (Fig. 1). The Juan de Fuca and Gorda ridges form the western boundary of the basin. The basin's eastern boundary is a subduction front between the North America and the Juan de Fuca plates. Sedimentologists have scrutinized the submarine fans and channel–levee complexes of Cascadia Basin (e.g., Griggs and Kulm 1970; Nelson 1976; Hampton et al. 1989; Adams 1990), but the distal edge of the depositional system remained poorly documented until site surveys were initiated for Leg 168 of the Ocean Drilling Program (ODP) (Davis et al. 1992). One of the primary objectives of Leg 168 was to quantify how basement topography, sediment thickness, and sediment permeability influence the thermo-physical characteristics of fluid circulation into and out of the igneous crust (Shipboard Scientific Party 1997a). A related goal was to pinpoint the circumstances under which fractured basalt is sealed off from hydrothermal exchange with ocean bottom water.

The Juan de Fuca plate is unusual because westward encroachment of a distal abyssal-plain facies has diminished ocean-crust fluid circulation close to the crest of the spreading ridge. Turbidites have been cored, in fact, within the axial valleys of the ridge (Normark et al. 1994; Zierenberg and Miller 2000). Sediment thickness increases toward the east as the Juan de Fuca plate approaches the subduction margin (Kulm and Fowler 1974; Carlson and Nelson 1987). At the subduction front, the plate-boundary fault passes through an abyssal-plain facies (Davis and Hyndman 1989). Material properties inherited from the distal edges of Cascadia Basin, therefore, affect the dynamics of subduction and frontal accretion (MacKay 1995; Underwood 2002).

As summarized by Mutti and Normark (1987), most turbidite basins fall into one of four categories: (A) old oceanic crust with large, long-lived sediment sources and little or no tectonic activity (e.g., Bengal, Amazon, Mississippi fans); (B) old oceanic crust with relatively long-lived sediment sources but with tectonic activity in the source basin transition area (e.g., Monterey and Astoria fans); (C) continental crust with relatively large and long-lived sediment supply but with structural control of basin configuration and duration (e.g., south-central Pyrenees and northern Apennines); and (D) continental crust where continuing tectonic activity results in relatively rapid changes in basin shape and short-lived sediment sources (e.g., California Continental Borderland). Turbidites are also common on the slopes of volcanic islands (e.g., Kelts and Arthur 1981; Hiscott et al. 1992; Garcia and Hull 1994).

Conversely, mid-ocean-ridge environments are usually immune to the input of siliciclastic turbidites because of their bathymetric height and long distance from terrigenous sediment sources. Because the Cascadia margin is active tectonically, its turbidite system is affected by the normal array of allocyclic forcing (i.e., uplift of coastal mountains, earthquakes, glacio-eustatic fluctuations, and explosive volcanic eruptions). In addition, mid-ocean-ridge volcanism and extensional faulting mold the seafloor architecture near the spreading center, thereby adding to the list of factors that affect sediment dispersal and facies architecture. The Cascadia sedimentary system, therefore, is in a class by itself.

The first purpose of this paper is to document the three-dimensional variability in turbidite stratigraphy along one portion of the Juan de Fuca Ridge flank (Fig. 1). We also present compositional data for the turbidites, interpret sediment provenance, identify regional-scale pathways of sediment dispersal, calculate long-term recurrence intervals for turbidity currents, and describe how textural variations between turbidites and interbeds of hemipelagic mud affect physical properties. We then show how the abyssal-plain facies of Cascadia Basin accelerates the hydrogeologic transition from open to sealed igneous basement. This feedback between sedimentation and fluid circulation has important global ramifications for thermal, chemical, and mechanical evolution of the ocean crust (Sclater et al. 1980; Alt et al. 1986; Fisher 1998), as well as ocean water chemistry (Mottl and Wheat 1994; Elderfield and Schultz 1996).

* Present address: Missouri Department of Natural Resources, Jefferson City, Missouri 65109, U.S.A.
** Present address: Sandia National Laboratories, P.O. Box 5800, Albuquerque, New Mexico 87185, U.S.A.
*** Present address: Department of Earth and Environmental Science, New Mexico Institute of Mining and Technology, Socorro, New Mexico 87801, U.S.A.

JOURNAL OF SEDIMENTARY RESEARCH, VOL. 75, NO. 1, JANUARY, 2005, P. 149–164
 1527-1404/05/075-149/$03.00 DOI 10.2110/jsr.2005.012

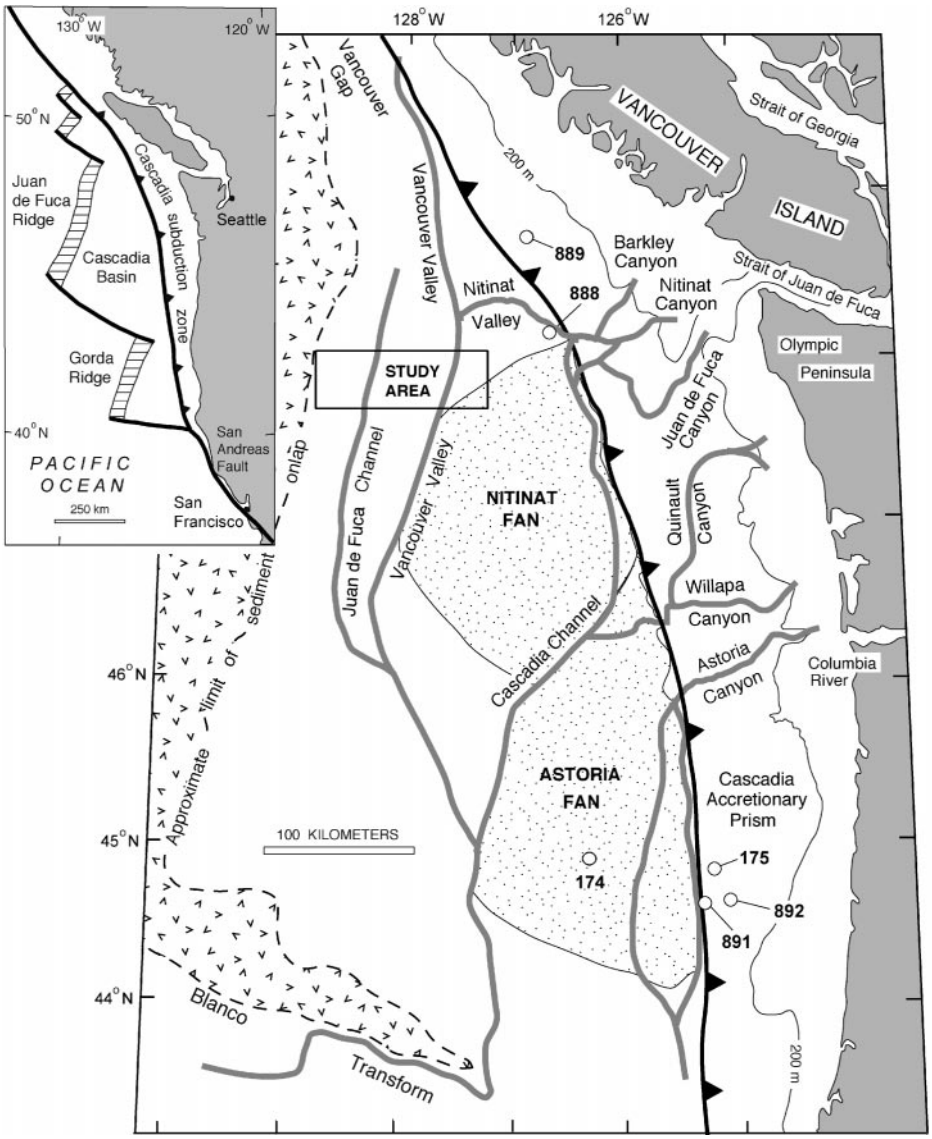

FIG. 1.—Physiography of the Cascadia Basin (after Karl et al. 1989), with location of ODP Leg 168 study area. Bold numbers refer to previous drill sites of the DSDP and ODP. Heavy line with teeth represents approximate position of the Cascadia subduction front. Inset map shows regional plate-tectonic context of Cascadia Basin.

GEOLOGIC AND OCEANOGRAPHIC SETTING

Depositional Character of Cascadia Basin

The floor of Cascadia Basin widens and slopes to the south (Fig. 1). The average seafloor gradient is 1:1000, and the maximum water depth is 2930 m. Submarine canyons function as the principal conduits for sediment transport across the continental margin (Herzer 1978; Davis and Hyndman 1989; Carson et al. 1986). The anastomosing network of Barkley, Nitinat, and Juan de Fuca canyons, for example, begins near the mouth of the Strait of Juan de Fuca (Fig. 1). Farther south, Willapa and Astoria canyons (Fig. 1) have connected directly to the Columbia River mouth during glacial lowstands (Carlson and Nelson 1969; Barnard 1978). During the Holocene highstand, the canyons have trapped fine-grained sediments and have helped focus sluggish downslope movement of the bottom nepheloid layer (Stokke et al. 1977).

Channel–levee complexes and submarine fans dominate the physiography of the basin floor (Griggs and Kulm 1970; Hampton et al. 1989; Karl et al. 1989). Vancouver Valley begins near 50°N at the shelf edge of northern Vancouver Island and merges with Juan de Fuca Channel near 46°N. Nitinat Valley intersects Vancouver Valley just north the Leg 168 study area (Fig. 1). Juan de Fuca Channel meanders from Queen Charlotte Sound through the northern portion of the basin (Carson 1973). Channels emanating from the mouth of the Barkley–Nitinat Canyon network branch off to the west and to the south to feed Nitinat Fan (Stokke et al. 1977; Shipboard Scientific Party 1994). Nitinat Fan reaches a maximum thickness of approximately 1500 m (Davis and Hyndman 1989). At ODP Site 888 (Fig. 1), on the northern fringe of Nitinat Fan, the total sediment thickness is approximately 2500 m (Shipboard Scientific Party 1994). Farther south, the channels of Astoria Fan radiate asymmetrically from the mouths of Astoria and Willapa canyons (Fig. 1). This turbidite system prograded at least 200 km to the south during the late Pleistocene (Carlson and Nelson 1969; Nelson et al. 1970; Nelson 1976). The distal part of the Astoria Fan was cored at DSDP Site 174 (Fig. 1), where total sediment thickness is approximately 910 m (Shipboard Scientific Party 1973).

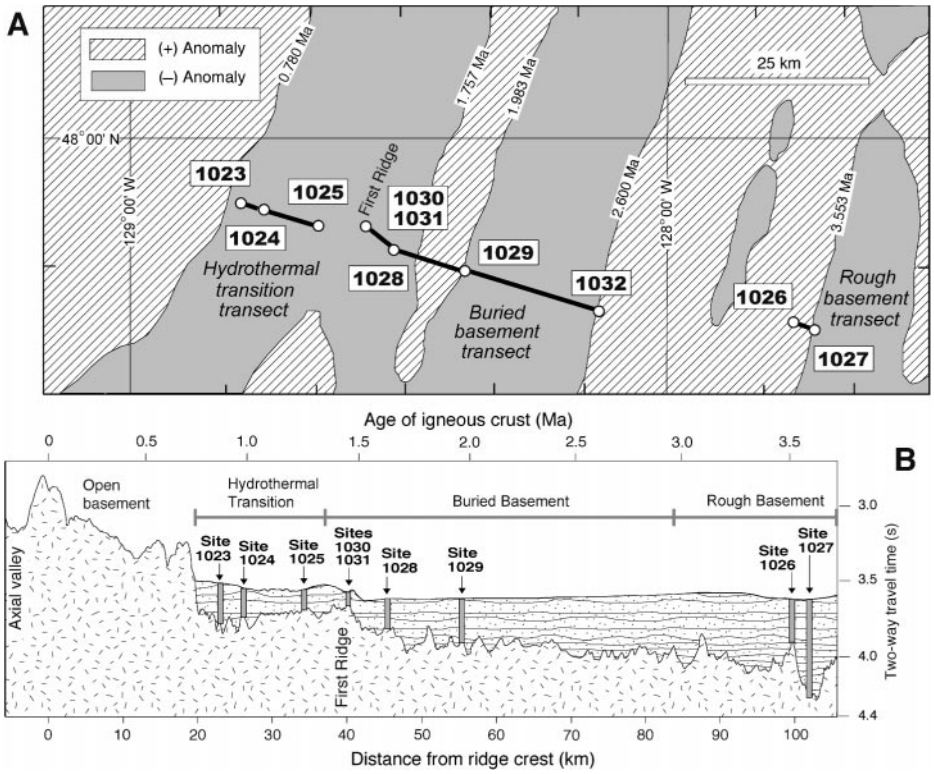

FIG. 2.—Magnetic-anomaly base map for Leg 168 study area with locations of drill sites assigned to the Hydrothermal Transition, Buried Basement, and Rough Basement transects (after Shipboard Scientific Party 1997a). Ages of magnetic polarity transitions are given in Ma. Cross section through drill sites shows how basement topography and sediment cover change across the eastern flank of the Juan de Fuca Ridge (after Shipboard Scientific Party 1997a). See Figure 1 for location of study area.

Stratigraphy of Leg 168 Drilling Sites

The nine sites of ODP Leg 168 form a transect that was divided into three parts (Fig. 2). Continuous coring utilized a combination of hydraulic piston corer, extended core barrel, and rotary coring systems. In general, three lithostratigraphic units combine to coarsen and thicken upward (Fig. 3). Unit thickness changes considerably from site to site, however, and nannofossil datums show most unit boundaries to be time transgressive (Shipboard Scientific Party 1997b, 1997c, 1997d; Su et al. 2000).

Beginning at the top of each section (Fig. 3), unit IA (sandy turbidite facies) contains hemipelagic mud and coarser interbeds that range from medium-fine sand to sandy silt and silt. Most of the sand and silt beds display sedimentary structures that are diagnostic of turbidites: sharp to erosional bases, normal size grading, plane-parallel laminae, ripple cross-laminae, and wavy to convolute laminae. The descriptive designation of mud as ''hemipelagic'' refers to its basic texture (silty clay to clayey silt) and mineral composition (mixture of biogenous and terrigenous constituents), rather than its mode of deposition. The mud is typically structureless to the naked eye, with scattered clay-rich bands, silt laminae, bioturbation, concentrations of calcareous nannofossils, and pyrite nodules. Muddy turbidite tops typically grade into the hemipelagic interbeds. Rigorous discrimination between hemipelagic and turbidite mud requires SEM analysis of grain fabric (Giambalvo et al. 2000) and/or statistical analysis of grain size distribution (Spinelli et al. 2004). The deepest discrete sand layer marks the base of unit IA. Below that boundary, thin interbeds of silt and hemipelagic mud typify unit IB (silty turbidite facies). Unit II is composed entirely of hemipelagic mud. The operational base of unit II generally coincides with the first recovery of basalt rubble. At Site 1027, however, a more complicated interval of basaltic talus, diabase sills, and hemipelagic mudstone separates unit II from highly fractured basalt basement.

The Hydrothermal Transition (HT) transect includes Sites 1023, 1024, and 1025 (Fig. 2). Located 20 to 35 km east of the volcanic axis of Juan de Fuca Ridge, this is the region where bare basement is first covered by terrigenous sediment (Fig. 2). Basement ages range from 0.860 Ma to 1.237 Ma (Fig. 3), and the wedge of sediment thickens from 97 to 192 m toward the spreading ridge. Seismic reflection profiles show small-scale levees and hummocks on the seafloor between Sites 1025 and 1024 (Fig. 4; Zühlsdorff and Spiess 2001). A relatively smooth basement surface dips toward the west, away from the crest of the first buried basement ridge (Fig. 4). The base of the sandy turbidite facies (unit IA) also increases in age toward the west from nannofossil zone 20 (0.28–0.46 Ma) at Sites 1024 and 1025 to zone 19 (0.46–0.76 Ma) at Site 1023.

The Buried Basement (BB) transect, 40 to 75 km east of the ridge axis, includes Sites 1028 through 1031 (Shipboard Scientific Party 1997d). Basement ages for these sites increase eastward from 1.615 Ma to 2.621 Ma (Fig. 3). For the most part, this region displays a basement surface that deepens to the east and is buried by thickening sediment. The base of unit IA occurs within nannofossil zone 20 (0.28–0.46 Ma), but the facies change is slightly older at Site 1029 than at Site 1028. Sites 1030 and 1031 are situated above a basement high that rises to within 41.3 m of the seafloor (Fig. 3). Sediment above this so-called ''first ridge'' consists of hemipelagic mud, carbonate-rich mud, and rare beds of silt to sandy silt.

The Rough Basement (RB) transect is located approximately 100 km east of the spreading axis, in an area that contains prominent linear basement ridges and troughs (Shipboard Scientific Party 1997c). Basement relief is typically 300 to 500 m (Fig. 2), and some basement highs pierce the sediment cover (Davis et al. 1992; Wheat and Mottl 1994; Mottl et al. 1998). Site 1027 is located above a basement trough, whereas Site 1026 is located over a buried ridge (Fig. 5). Their respective basement ages are 3.586 and 3.511 Ma (Fig. 3). At Site 1026, the shift from silty to sandy turbidites occurs within nannofossil zone 19 (0.46–0.76 Ma); the same

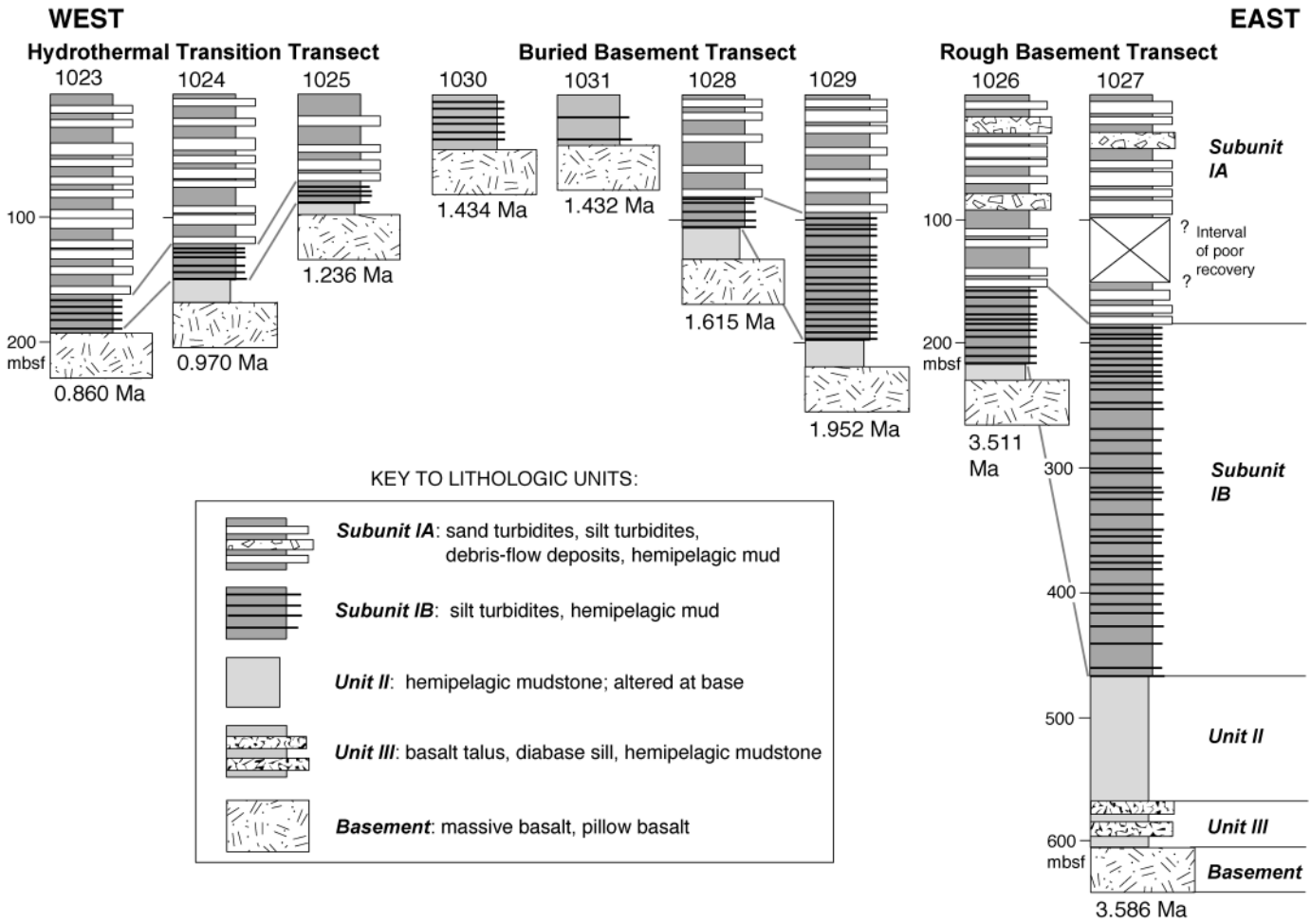

FIG. 3.—Lithostratigraphy of the Leg 168 drill sites. Ages of basaltic basement (from Shipboard Scientific Party 1997a) are in Ma.

facies boundary at Site 1027 is within zone 20 (0.28–0.46 Ma). Seismic reflection profiles show geometric manifestations of a buried channel, as well as an interval of discontinuous reflectors from roughly 3.70 to 3.76 s two-way travel time (Fig. 5). That acoustic interval coincides with a zone of no core recovery (87 to 145 mbsf) where the sediment is probably sandy (Fig. 3). The thickest sand bed above the no-recovery interval is 7 m. The deepest silt turbidites appear at 216.13 mbsf in Hole 1026C ($\sim$ 1.15 Ma) and at 466.95 mbsf in Hole 1027B ($\sim$ 1.68 Ma).

LABORATORY METHODS

Conventional ODP core descriptions were augmented by visual logging of all sand and silty-sand layers that exceed 1 cm in thickness. The archive half of each section was used to locate each turbidite base (in meters below seafloor) and to estimate bed thickness. Diffuse boundaries between muddy turbidite tops and interbeds of hemipelagic mud result in underestimates of true turbidite thickness. Sediment index properties (bulk density, water content, porosity, and void ratio) were measured aboard the *JOIDES Resolution* following conventional protocols (Shipboard Scientific Party 1997b; 1997c; 1997d). A SediGraph 5000ET analyzer (Jones et al. 1988; Stein 1985: Singer et al. 1988) was used to obtain grain size data (see Cavin et al. 2000, for description of sample preparation).

Disaggregated sand samples (> 63 μm) were processed for petrography according to methods described by Underwood and Hoke (2000). Epoxy grain mounts were ground to standard thin sections and stained for easier identification of plagioclase and potassium feldspar (Houghton 1980). We used the Gazzi–Dickinson point-counting method, whereby all sand-size crystals are assigned to their respective mineral categories, even if they occur in polycrystalline rock fragments (Dickinson 1970; Ingersoll et al. 1984). Saettler (1998) counted at least 500 grains per thin section. Grain types were assigned to 22 categories before combining into the following monocrystalline and polycrystalline modes: Q = total quartz; Q_p = polycrystalline quartz; Q_m = monocrystalline quartz; F = total feldspar; P = plagioclase feldspar; K = potassium feldspar; L = total unstable-lithic fragments; L_s = sedimentary-lithic fragments; L_v = volcanic-lithic fragments; L_m = metamorphic-lithic fragments; L_{sm} = sedimentary- and metasedimentary-lithic fragments. Saettler (1998) also separated volcanic-rock fragments into three broad categories (V_b = basaltic, V_a = andesitic, and V_r = rhyolitic), on the basis of texture and mineral composition. Rhyolitic grains display granular or seriate mosaics of interlocking quartz, K-feldspar, and plagioclase crystals. Andesitic grains show a variety of microlitic textures, with euhedral and twinned lathes of plagioclase in a groundmass of glass or altered glass. Basaltic grains typically have heavily altered groundmass, lathework textures, microcrysts of plagioclase, and minor amounts of olivine and/or pyroxene.

RESULTS

Turbidite Stratigraphy

The first thing to consider in the time-transgressive stratigraphy of Cascadia Basin is the initiation of sedimentation above basalt. The sediment–

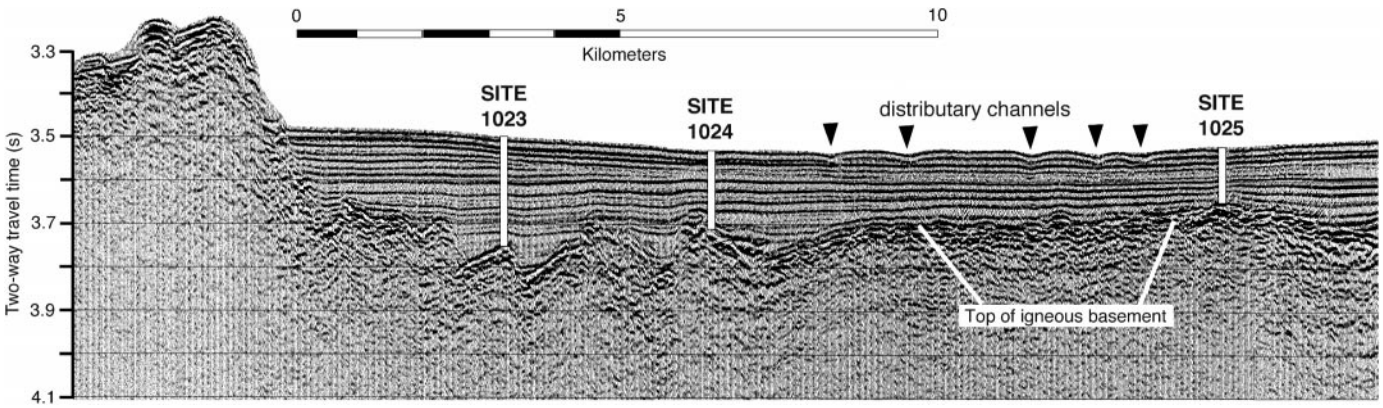

FIG. 4.—Seismic reflection profile through ODP drilling sites of the Hydrothermal Transition (1023, 1024, and 1025) (from Shipboard Scientific Party 1997b). Note the irregular morphology of the seafloor created by small channels.

basalt contact and the first occurrence of turbidites both increase in age from west to east. Nannofossil ages (Su et al. 2000) show that hemipelagic deposition began at Site 1027 soon after basement formed at 3.586 Ma (Fig. 3). Initially, this basement trough filled slowly by fall-out of suspended mud (accumulation rate = 10.19 cm/Ky). As basement obstructions to the east and north were buried, the first silty turbidity currents arrived at ~ 1.6 Ma. By 1.1 Ma, subsidence was sufficient, and enough sediment had filled the valley, for silty turbidites to encroach upon the nearby ridge at Site 1026. Farther west, at Sites 1029 and 1028, initiation of silty turbidite deposition was delayed until approximately 0.9 Ma. Basement beneath Sites 1030 and 1031 remained high enough to prevent turbidity currents from spilling over into the area of the HT transect until ~ 0.46 Ma (Shipboard Scientific Party 1997b).

Average rates of accumulation within the sandy turbidite facies (uncorrected for compaction) range from 11.83 cm/ky to 55.88 cm/ky (Su et al. 2000). To compare recurrence intervals for delivery events, we subdivided the record into four time-stratigraphic periods common to all three transects, as constrained by nannofossil datums: period A = less than 0.09 Ma, period B = 0.09–0.28 Ma, period C = 0.28–0.46 Ma, and period D = 0.46–0.76 Ma. Because core recovery was less than 100% (Shipboard Scientific Party 1997b, 1997c, 1997d), these statistics provide minimum estimates for the number of events during a given time period and the average interval of recurrence (RI) between those events.

Within the HT transect, the upper part of the seismic section shows a clear eastward decrease in sediment thickness above the west-dipping basement (Fig. 4). The average time between turbidite events increases in the same direction (Fig. 6). Within period A at Site 1023, at least 133 turbidites were deposited (RI = 676 yr), whereas Sites 1024 and 1025 contain only 71 and 6 deposits, respectively. Period B included at least 171 turbidites at Site 1023 (RI = 1111 yr) but only 117 at Site 1024 (RI = 1624 yr) and 97 at Site 1025 (RI = 1959 yr). The spatial pattern for period C is just the opposite, however, with the number of turbidites increasing substantially from west to east (Fig. 6).

Turbidite records within the Buried Basement transect show substantial discrepancies between Sites 1028 and 1029 even though basement relief was buried completely during the four time-stratigraphic periods in question (Fig. 7). Shorter recurrence intervals switch back and forth, and there are also substantial differences in turbidite thickness. At least 108 turbidites were deposited at Site 1028, for example, within period A (RI = 833 yr), whereas Site 1029 contains only 38 (RI = 2368 yr). Thicker turbidites (> 20 cm) are common only in the upper 15 m of Hole 1028A, whereas Site 1029 displays a higher proportion of thick beds and shorter recurrence interval (RI = 984 yr) within the strata of period C.

Sites 1026 and 1027 (RB transect) also display considerable differences in turbidite records (Fig. 8) despite their close spacing (Fig. 5). During period A, the number of turbidites increased from 41 at Site 1026 (RI = 2195 yr) to 61 at Site 1027 (RI = 1475 yr). Thicker beds are common within interval B at Site 1026, where the recurrence interval is 1080 yr. We were unable to identify the equivalent record at Site 1027 because of poor core recovery within the seismically complex zone from 90 to 145 mbsf (Fig. 5). We interpret this acoustic interval as a major episode of channel infilling. Periods C and D at both sites show RI values longer than most at the HT and BB transects (Fig. 8).

Physical Properties

Cavin et al. (2000) tabulated the results of grain size analyses and correlated the data with shipboard measurements of index properties (Shipboard Scientific Party 1997b, 1997c, 1997d). Contents of clay-size particles in hemipelagic and turbidite mud are typically between 60% and 85% for each lithostratigraphic unit, and mean grain size averages 2 to 3 μm. Values of water content, porosity, and void ratio generally increase with increasing clay content, whereas bulk density tends to decrease with higher proportions of clay. There is a noticeable separation of data from mud samples (both hemipelagic and turbidite) and data from sand and silt beds (Fig. 9). Variability is largest within the upper 100 to 150 m, where porosity values range from 80% to 30% (Fig. 10A). After segregating according to lithology, two compaction trends emerge (Fig. 10B, C). The initial porosity values tend to be significantly lower for sand and silt (35% to 55%) than for hemipelagic and turbidite mud at comparable depths (50% to 80%). Moreover, there is minimal dewatering in the sand layers over a depth range of 0–120 mbsf. Conversely, mud porosity near the seafloor is usually greater than 70%, and values drop to ~ 40% at depths below 500 mbsf. Data from the mud samples fit an exponential compaction curve to depths of ~ 200 mbsf. Below 200 mbsf, a linear trend provides a better fit to the mud compaction (Fig. 10A).

Sites 1030 and 1031 are unusual because total sediment accumulation rises only ~ 45 m above basement and mud porosity remains high (65–80%) throughout the section (Fig. 10D). The textural characteristics of those muds appear to be no different than those of hemipelagic deposits elsewhere (Cavin et al. 2000; Giambalvo et al. 2000). Analyses of porewater chemistry, however, show clear evidence of upward fluid flow from igneous basement through the mud blanket (Shipboard Scientific Party 1997d).

Sand Petrography

One hundred and thirty-four thin sections were analyzed by point counting (for data tables, see Underwood and Hoke 2000). The proportions of total quartz, total feldspar, and lithic fragments (Q-F-L) within the HT

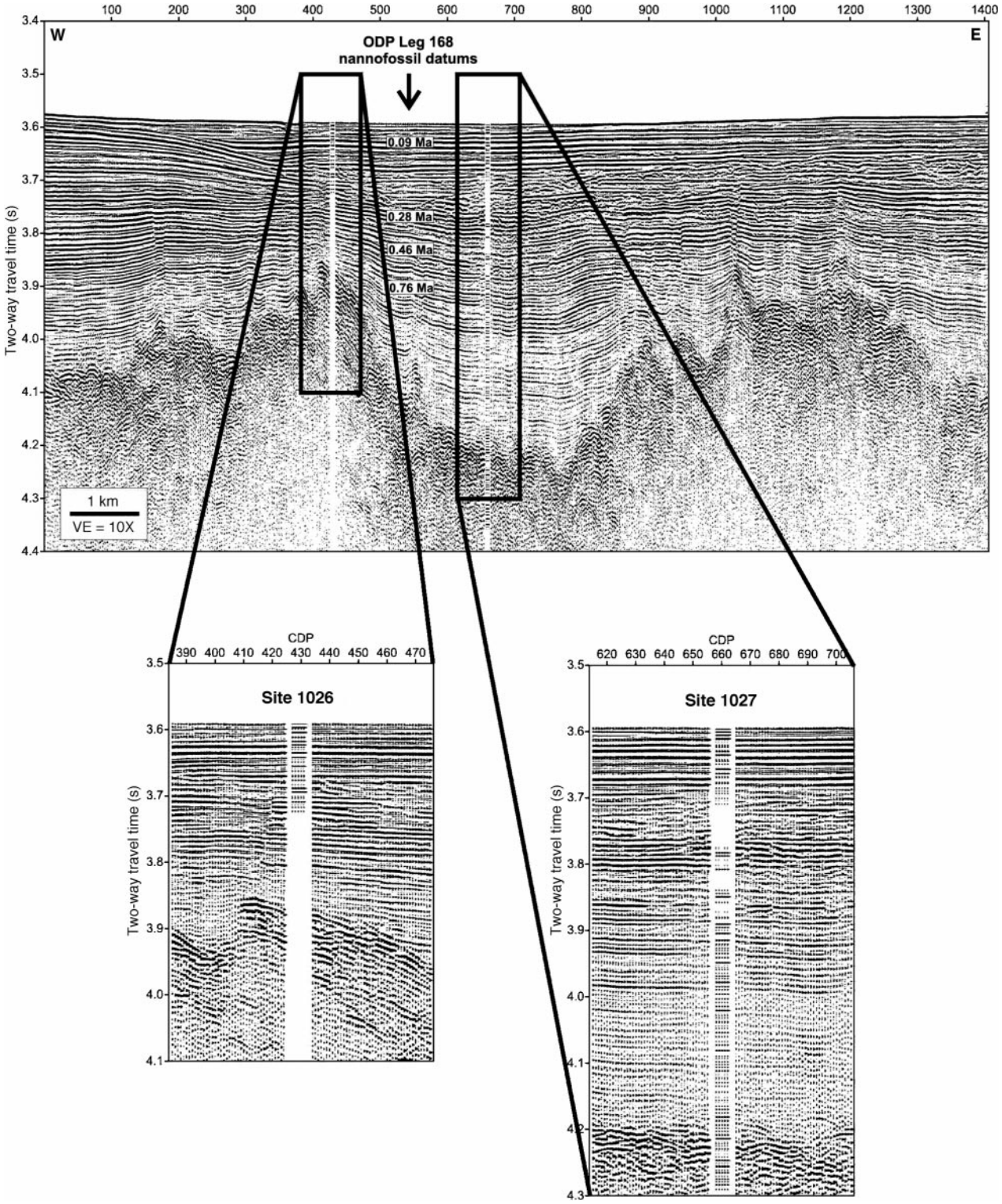

FIG. 5.—High-resolution seismic-reflection profile through ODP Sites 1026 and 1027, Rough Basement transect. These data were shot after the sites were drilled. Enlargements show details of synthetic seismic responses that were calculated from core density logs (see Zuehlsdorff and Spiess 2001 for details). Approximate positions of nannofossil datums between drill sites are based on Su et al. (2000).

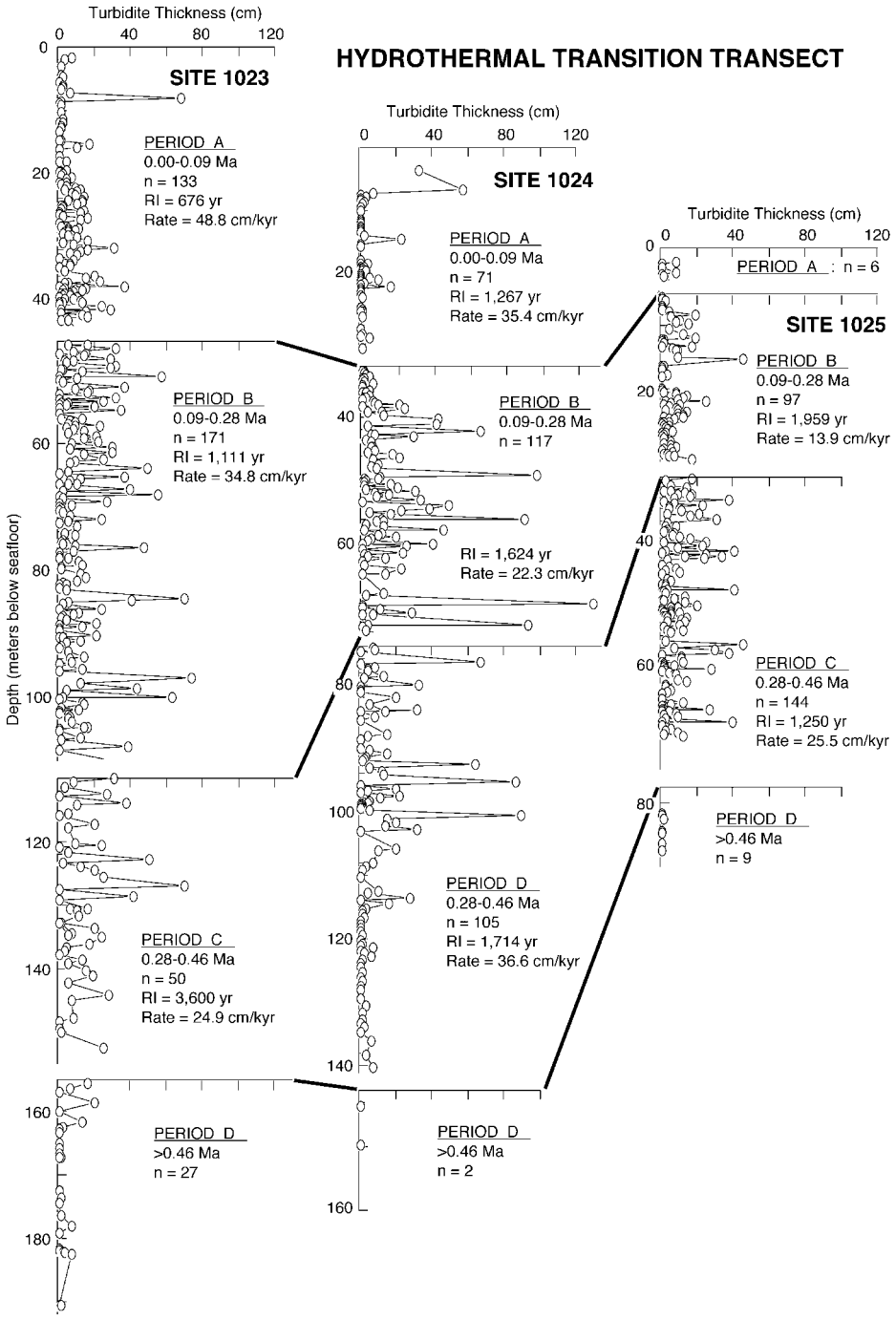

FIG. 6.—Number of turbidites (n) and turbidite recurrence intervals (RI) for the Hydrothermal Transition transect, ODP Sites 1123, 1124, and 1125. Age constraints for each time interval (Ma) are from Su et al. (2000). Rates of sediment accumulation (cm/kyr) have not been corrected for compaction.

transect are approximately equal in most samples (Fig. 11), and temporal variations are modest. The average proportions of volcanic grain types for the HT transect are: Site 1023 $V_r = 36$, $V_a = 38$, $V_b = 26$; Site 1024 $V_r = 32$, $V_a = 47$, $V_b = 21$; Site 1025 $V_r = 40$, $V_a = 42$, $V_b = 18$. One exception to this homogeneity is the occurrence of sandy silt layers in the lower part of unit IA and from unit IB that contain over 75% of what we interpret to be intraformational mud chips (Fig. 12). The sand-size mudstone particles are typically brownish-yellow in color and contain silt-size grains of monocrystalline quartz, plagioclase, calcite, microfossils, opaque grains, mica, and mafic minerals in a clay matrix. These clasts probably were remobilized off adjacent basement highs.

Sand samples from Sites 1028 and 1029 (BB transect) are also homogeneous in Q-F-L modes (Fig. 11), but their variations in polycrystalline constituents are larger and more erratic than those from the HT transect (Fig. 12). Overall, the proportions of L_v and L_{sm} increase down-section. The average proportions of volcanic grain types are $V_r = 28$, $V_a = 44$, $V_b = 28$ for Site 1028 and $V_r = 33$, $V_a = 42$, and $V_b = 24$ for Site 1029. In the RB transect, polycrystalline quartz and volcanic-rock frag-

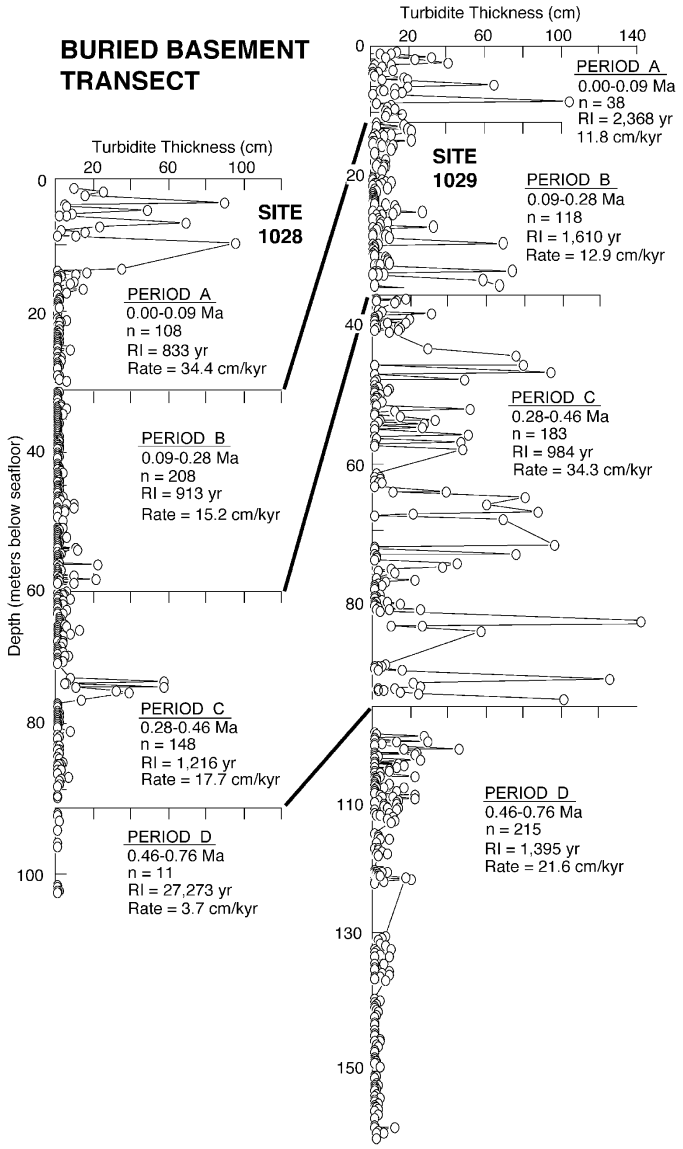

FIG. 7.—Number of turbidites (n) and turbidite recurrence intervals (RI) for the Buried Basement transect, ODP Sites 1128 and 1129. Age constraints for each time interval (Ma) are from Su et al. (2000). Rates of sediment accumulation (cm/kyr) have not been corrected for compaction.

ments at Site 1026 increase steadily above the 0.28 Ma datum, whereas sedimentary-rock plus metamorphic-rock fragments decrease upsection from 75% to 27% (Fig. 12). These trends, however, are not apparent at Site 1027. Above the 0.09 Ma datum, Sites 1026 and 1027 show small but consistent increases in sedimentary plus metamorphic-rock fragments (Fig. 12). The average volcanic-rock proportions are $V_r = 27$, $V_a = 44$, $V_b = 29$ for Site 1026 and $V_r = 30$, $V_a = 44$, $V_b = 26$ for Site 1027.

DISCUSSION

Sediment Compaction and Hydrogeology

Differences in depositional processes and accumulation history between the Leg 168 sites imparted concomitant variations in sediment compaction and dewatering. Initial porosity values for true hemipelagic mud (i.e., products of slow deposition by vertical settling) are significantly higher than values for the muddy tops of turbidites, even though their color, visual

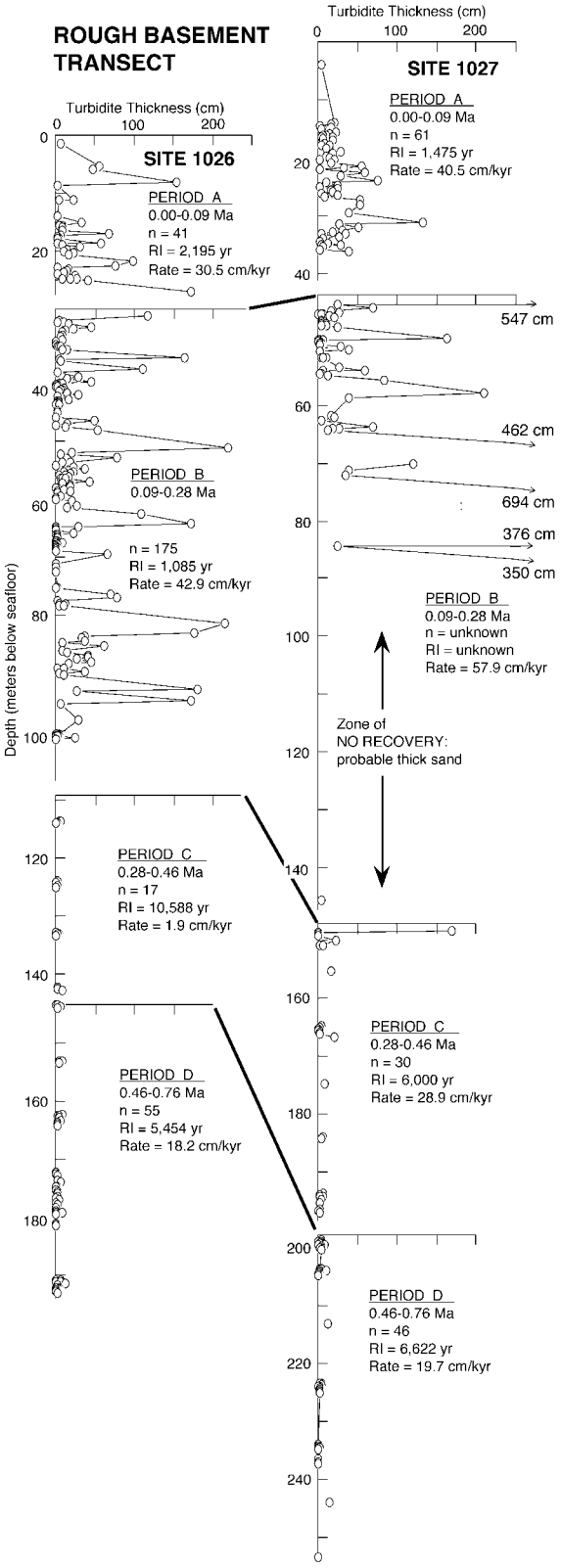

FIG. 8.—Number of turbidites (n) and turbidite recurrence intervals (RI) for the Rough Basement transect, ODP Sites 1126 and 1127. Age constraints for each time interval (Ma) are from Su et al. (2000). Rates of sediment accumulation (cm/kyr) have not been corrected for compaction.

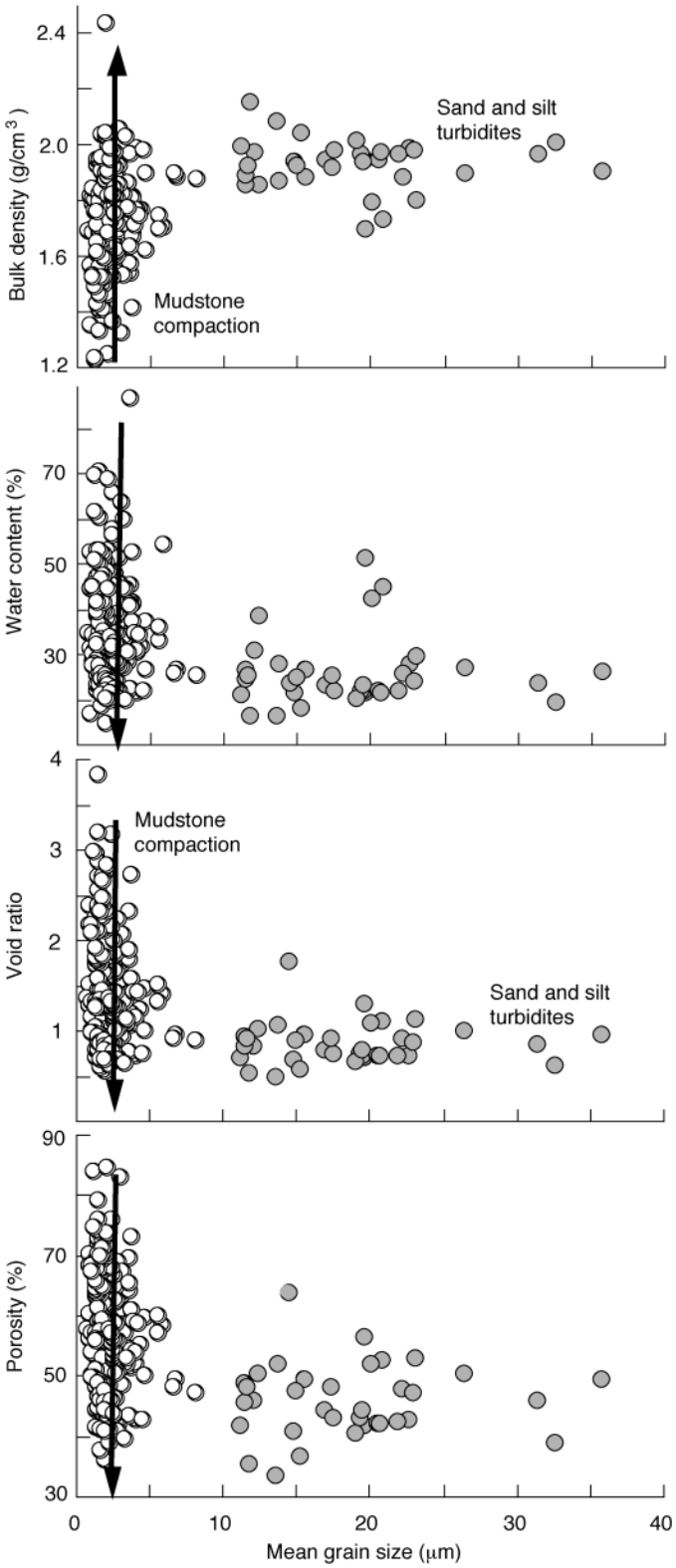

FIG. 9.—Cross plots of mean grain size (μm) versus index properties of sediment (bulk density, porosity, void ratio, and water content) as determined by shipboard measurements of samples from all sites cored during Leg 168 (Shipboard Scientific Party 1997b, 1997c, 1997d). Values of mean grain size are based on quartile measures and apply only to the size fractions ($<$ 63 μm) that were analyzed by SediGraph (see Cavin et al. 2000). Note the separation of compaction responses for sand and silt turbidites versus hemipelagic and turbidite muds.

texture, mean grain size, and bulk mineralogy are indistinguishable (Giambalvo et al. 2000). The hemipelagic mud contains more foraminifers relative to turbidite mud, and their grain orientations are random to subvertical as revealed by scanning electron microscopy. Random grain orientations are indicative of settling as fecal pellets and/or flocculated aggregates. In contrast, the turbidite muds show systematic bed-parallel alignment of phyllosilicates in response to bed-parallel shear during the waning stages of gravity flow. Statistical distributions of grain size also differ between the hemipelagic and turbidite muds (Spinelli et al. 2004). The interdigitation of two mud types with contrasting initial grain fabrics helps to explain why porosity values are so scattered within the upper 150 m of each sediment column (Fig. 10B).

One of the more dynamic aspects of the mid-ocean ridge-flank environment is the shift from a hydrologically open basement to a sediment-sealed basement. The resistance of sediment's intergranular pore space to fluid flow controls the degree to which the underlying basalt and the overlying ocean remain physically and chemically coupled (Karato and Becker 1983; Fisher et al. 1994; Snelgrove and Forster 1996). The vigor of this hydrologic coupling affects many important processes: the transition from advective to conductive heat flow (Sclater et al. 1976; Stein and Stein 1994); the nature of hydrothermal alteration of the crust (Alt et al. 1986); the evolution of such crustal properties as seismic velocity (Jacobson 1992); and the oceanic mass balance of reactive elements such as magnesium (Mottl and Wheat 1994).

With one exception (Site 1027), the sediment in contact with Juan de Fuca igneous basement is hemipelagic mud (unit II). Samples of hemipelagic mud possess lower permeability at a given porosity than do muddy turbidites (Giambalvo et al. 2000; Spinelli et al. 2004). The compression index (i.e., the slope of the virgin consolidation curve) also increases with the proportion of hemipelagic material. As the total sediment column gradually thickens above the basalt, compaction transforms the basal sediment layer from a highly porous mud into an increasingly impermeable aquitard. We know from geochemical evidence that the upflow of fluids remains active today at Sites 1030 and 1031, at calculated rates of 1.9 to 3.2 mm/yr (Shipboard Scientific Party 1997a; Giambalvo et al. 2002). Seepage rates calculated from piston-core data are 0.15–7.0 mm/yr over the ridge crest, as compared to 0.06–0.10 mm/yr off the ridge crest where total sediment is thicker and turbidites are more common (Spinelli et al. 2004). Thus, the spatial extent and rate of seepage near basement highs change as a function of both sediment thickness and sediment type.

Several factors need to be considered when assessing fluid flow near the ridge flank. High-resolution seismic reflection data show narrow zones of acoustic blanking (decreased reflection amplitudes) that are manifestations of higher porosity (Züehlsdorff et al. 1999). The blanking zones are probably local products of basement-related fault-bend folding (Züehlsdorff and Spiess in press). Outside of such zones, the driving force for fluid seepage through the sediment appears to be excess pore pressure (i.e., greater than hydrostatic) within the highly fractured upper basement (Giambalvo et al. 2000; Spinelli et al. 2004). It is difficult to determine exactly when the effects of increasing burial reduce the flow rate to insignificant levels, but the total overburden at Sites 1030 and 1031 ($<$ 45 m) is obviously not thick enough to stop flow. Porosity values at the two sites where seepage is still occurring are higher (by $\sim$ 7%) than values for either turbidite or hemipelagic muds at the same range of depths ($<$ 45 mbsf) at the seven sites without fluid seepage (Fig. 10D). Thus, some factor (or factors), in addition to overburden pressure, must affect the flow rate. The random grain fabric in a uniform hemipelagic section should lead to initial conditions with higher porosity; stratigraphic compartments with mostly hemipelagic mud, therefore, might act as preferred zones for pressure-driven upflow. Reductions of pore pressure and porosity collapse, in turn, translate into a 10$\times$ to 100$\times$ decrease in permeability as one moves from the crest of the buried ridge (with its thinner hemipelagic apron) to the flanks of the basement high (thicker sediment, more turbidites) (Spinelli et al. 2004).

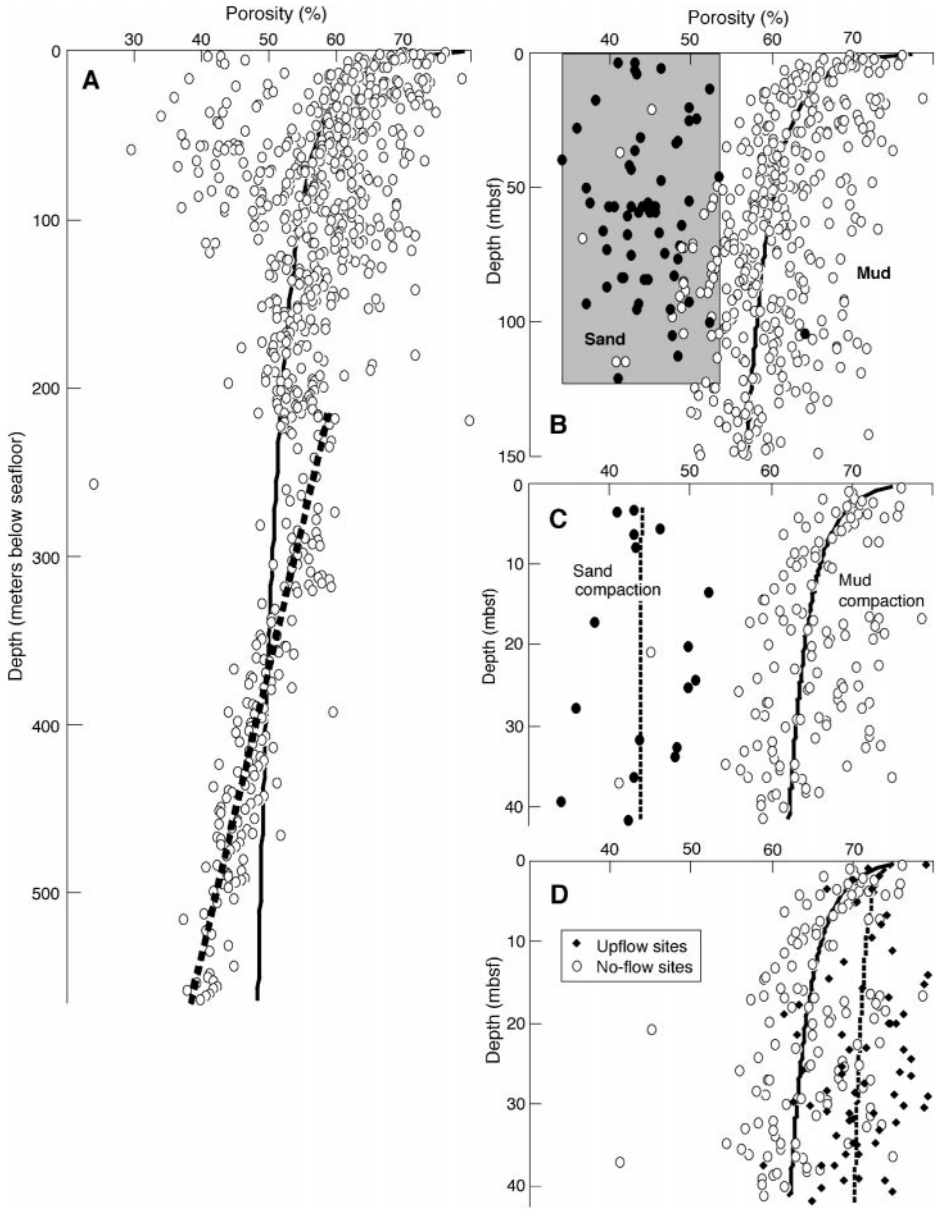

FIG. 10.—Depth profiles of sediment porosity as determined by shipboard measurements of samples from all sites cored during Leg 168 (Cavin et al. 2000). **A)** Complete compilation of data from no-flow sites (Sites 1023 through 1029), without segregation by lithology. A single compaction curve follows the form $n = az^b$. Note the shift to a linear compaction gradient at ~ 200 mbsf. **B)** Comparison of porosity trends for turbidite sand and hemipelagic or turbidite mud lithologies within the upper 150 m at the no-flow sites. Turbidite sands become increasingly sparse below 120 mbsf. **C)** Comparison of porosity trends for sand and mud lithologies within the upper 42 m at the no-flow sites. **D)** Comparison of porosity trends for mud lithologies within the upper 42 m at the upflow sites (Sites 1030 and 1031) vs. the no-flow sites. The upflow sites contain mostly hemipelagic mud, whereas the no-flow sites at the same depths contain both hemipelagic and turbidite mud. Compaction curves for the two data sets show a shift of ~ 7% porosity.

Thus, the same zones where initial conditions favor upflow also tend to sustain higher permeabilities for longer periods of time.

Numerical modeling demonstrates that hemipelagic mud in unit II should maintain geochemically detectable flow (> 0.1 mm/yr) up to a threshold burial depth of 150 mbsf, assuming an overpressure of 5 kPa above hydrostatic (Giambalvo et al. 2000). This threshold value is close to an estimate of 160 m that was derived independently by Wheat and Mottl (1994). At each of the Leg 168 sites without seepage, the accumulation of turbidites has resulted in burial of unit II to depths of 100–150 mbsf. The texture, grain fabric, and permeability of the Cascadia turbidites probably do not influence the behavior of ocean-crust hydrology and hydrothermal circulation. The turbidite section does play an important indirect role, however, by rapidly increasing the lithostatic load above the basal layer of hemipelagic mud, thereby accelerating the transformation from open to sealed basement through sediment compaction and grain-fabric collapse.

Evolution of Turbidite Systems on the Ridge Flank

Stratigraphic correlation of turbidites can be straightforward if such criteria as color, texture, geochemical composition, or fossil assemblages are distinctive enough (e.g., Pilkey et al. 1980; Pearce and Jarvis 1992; Weaver et al. 1992). Such is not the case for depositional sites on the eastern flank of the Juan de Fuca Ridge. Important factors within the basin include thermal subsidence of the lithosphere, normal faulting, constructional mid-

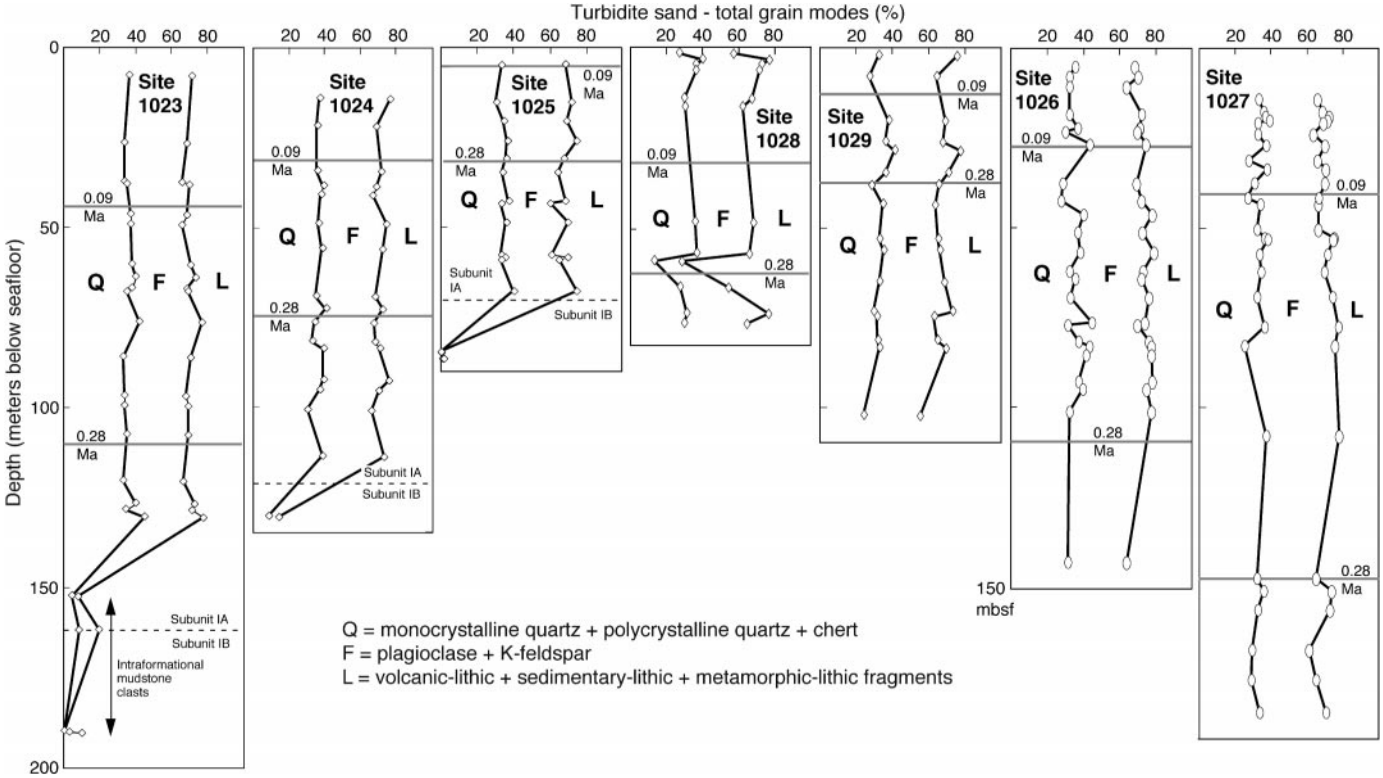

FIG. 11.—Depth variations in total detrital modes for turbidite sands from the Leg 168 drilling sites. Dashed lines with numbers are ages (in Ma) of nannofossil datums (From Su et al. 2000). Q = total quartz; F = total feldspar; L = unstable lithic fragments. See Underwood and Hoke (2000) for data tables.

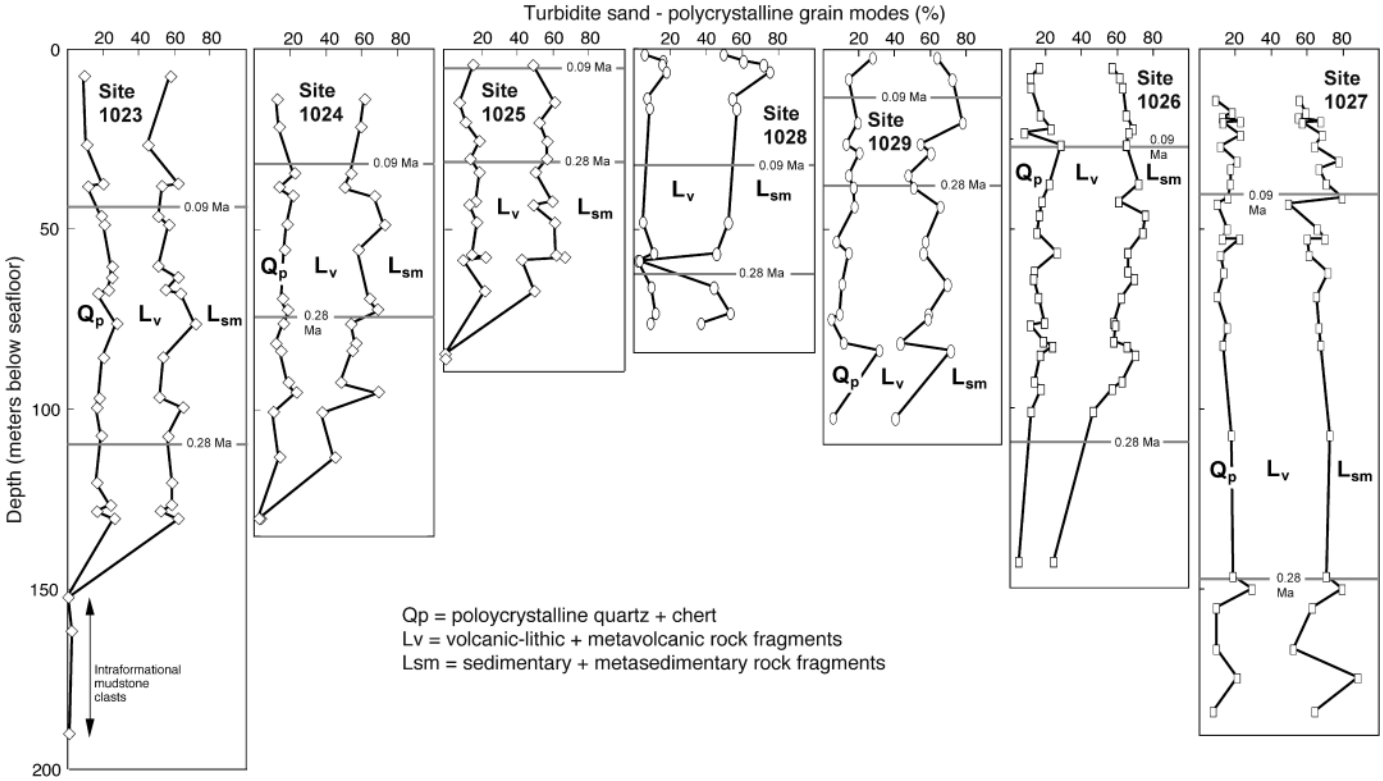

FIG. 12.—Depth variations in polycrystalline detrital modes for turbidite sands from the Leg 168 drilling sites. Dashed lines with numbers are ages (in Ma) of nannofossil datums (From Su et al. 2000). Q_p = polycrystalline quartz; L_v = volcanic-rock fragments; L_{sm} = sedimentary-rock and metasedimentary-rock fragments. See Underwood and Hoke (2000) for data tables.

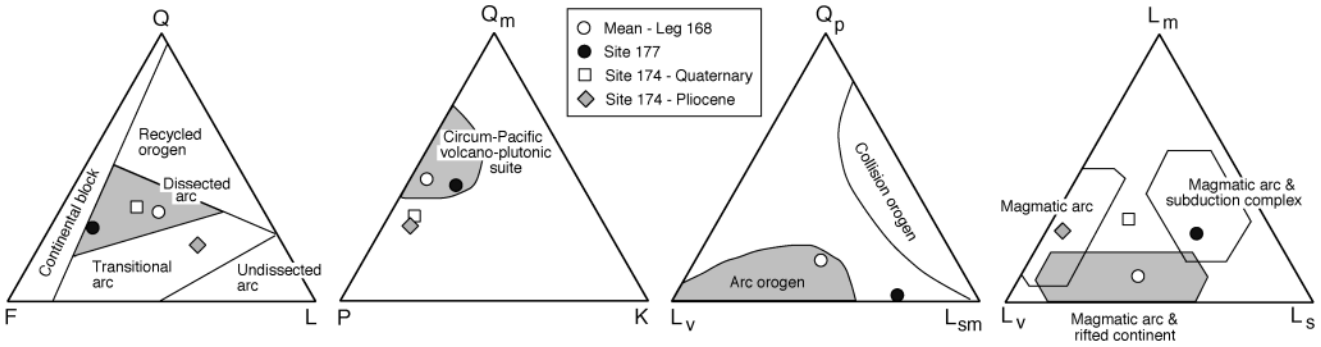

FIG. 13.—Ternary diagrams showing a comparison among mean detrital modes for sand deposits from the Leg 168 study area (Saettler 1998), Site 174 of the DSDP (Gergen and Ingersoll 1986; Marsaglia and Ingersoll 1992), and Site 177 of the DSDP (Gergen and Ingersoll 1986). Q = total quartz; F = total feldspar; L = unstable lithic fragments; Q_m = monocrystalline quartz; P = plagioclase; K = potassium feldspar; Q_p = polycrystalline quartz; L_v = volcanic-rock fragments; L_{sm} = sedimentary-rock and metasedimentary-rock fragments; L_m = metamorphic rock fragments. Boundaries for tectonic provenance fields are from Dickinson and Suczek (1979), Dickinson et al. (1983), and Ingersoll and Suczek (1979).

ocean-ridge volcanism, and the tendency of sediment gravity flows to funnel between or deflect around bathymetric obstructions. The three-dimensional shape of the seafloor changed dramatically during the past 3.5 My as juvenile lithosphere subsided and moved away from the spreading center. As each basement low filled with sediment, gradual smoothing of the seafloor reduced the severity of the landscape as a control on the pathways of unconfined sheet flows and channel–levee complexes. This dynamic balance between sedimentation and submarine geomorphology helps account for the large spatial and temporal differences in total accumulation rates between the Leg 168 drill sites.

Our comparison of sites shows that turbidite delivery to the northwestern edge of Cascadia Basin shifted in unpredictable ways. Working on a finer time scale, Carson and McManus (1971) encountered similar complications when they tried to correlate individual turbidites in nearby piston cores. At the resolution of piston cores, channel environments produce small-scale (1–2 km) horizontal facies changes that are more abrupt than those in interchannel environments. This type of contrast is also clearly evident from seismic-reflection profiles of buried channels within the RB transect (Fig. 5). Over longer time periods, depocenters shifted substantially in response to channel migration, overbank flooding, and channel avulsion or abandonment. The most vigorous phase of sand deposition occurred at Site 1027 during the interval between 0.28 and 0.09 Ma (Fig. 8), when a channel–levee complex of substantial size (proto–Vancouver Valley) flowed through the RB transect area. Rates of sedimentation have decreased within that locality over the course of the past 90,000 years.

Migration of depositional centers near the Juan de Fuca Ridge did not follow a simple pattern of east-to-west progradation and onlap. Within the HT transect area, for example, rates of turbidite sedimentation increased up-section at Sites 1023 and 1024 but decreased up-section at Site 1025 (Fig. 6). The shortest recurrence interval for turbidity currents within the RB transect (Fig. 8) occurred within time period B (0.09–0.28 Ma), whereas the most rapid infilling of the BB transect area (Fig. 7) took place earlier during period C (0.28–0.46 Ma). The shortest recurrence interval was 676 years (period A at Site 1023), but in most cases the average frequency of occurrence was one turbidite every 1000 to 2000 years. The shorter RI statistics compare reasonably well with data from the more proximal parts of Cascadia Basin, which has been affected by 13 turbidity currents (Adams 1990) since deposition of the Mazama ash layer approximately 7600 years ago (Zdanowicz et al. 1999). During the Holocene highstand of sea level, large subduction-related earthquakes have provided the main triggering mechanism for turbidity currents (Adams 1990). During Pleistocene lowstands and early stages of deglaciation, however, canyon heads and shelf environments almost certainly were affected by other triggers, including large storm waves, seaward-directed storm surges (e.g., Nelson 1982; Duke 1985), and hyperpycnal discharge from rivers, glaciers, and glacial lakes (e.g., Mulder and Syvitski 1995).

Another contributing factor might have been occasional reflection or remobilization of gravity flows off the nearby ridges. In some instances, flow reflection probably resulted in duplication of sand and silt deposits during a single transport event. The effect of seafloor relief on the dynamics of a turbidity current is impossible to predict or model in detail without knowing the corresponding values of all of the governing physical parameters (i.e., speed, direction, three-dimensional density gradient, thickness, frictional coefficients, seafloor gradient). The ability of any individual turbidity current to flow over the top of a bathymetric obstruction is dictated largely by the relation between flow thickness and ridge height. To a first approximation, numerical and laboratory models indicate that the maximum elevation of upslope flow (i.e., a true vertical shift in center of gravity for a flow of uniform density) is 1.5 times the flow thickness (Muck and Underwood 1990; Kneller and Buckee 2000). More rigorous solutions require complex integration of velocity and density profiles within turbid flows (Kneller and McCaffrey 1999). In other settings worldwide, deposits of turbidite sand have been documented at elevations several hundred meters above abyssal floors (e.g., Damuth and Embley 1979; Dolan et al. 1989; Garcia and Hull 1994). Where ridge height exceeds vertical run-up, all or part of the turbidity current should be deflected or reflected by the obstruction (Pantin and Leeder 1987; Kneller et al. 1991; Pickering et al. 1992; Kneller and McCaffrey 1999). Conversely, if a flow is thicker than the ridge is high, the process of flow stripping should detach the entrained layer and allow bypassing (Piper and Normark 1983; Alexander and Morris 1994). In applying these concepts to Cascadia, each of the turbidity currents must have adjusted differently to the rugged landscape of its flow path, under a unique set of flow parameters, while moving toward the distal edge of the basin. The net result is unusually patchy and unpredictable turbidite architecture.

Integration of high-resolution seismic reflection data, core data, and synthetic seismics provides additional evidence for shifts in turbidite input and accumulation rate (Zühlsdorff and Spiess 2001). The facies change between units IA and IB, for example, differs in age from site to site and cannot be matched to a single seismic reflector. Changes in reflection amplitude indicate a gradual decrease in grain-size contrasts from Site 1024 toward Site 1025, consistent with the upper two intervals of the coring record. In general, reflection character is more uniform within younger parts of the seismic section, but Zühlsdorff and Spiess (2001) could trace only one reflector (‘‘reflector A’’) across the first basement ridge (i.e., from Site 1025 to the BB transect). The estimated depth of that reflector is 21 m at Sites 1024 and 1025, and 25 m at 1028. This interpretation is at odds, however, with the biostratigraphic data of Su et al. (2000), which place the

TABLE 1.—*Mean detrital modes for Leg 168 sites and potentially correlative sand deposits within Cascadia Basin and related watersheds.*

Location	Mean Q-F-L	Mean Lv-Ls-Lm	Size (mm)	Count Method*	Stain**	Density***	Source
ODP Leg 168 sites	35-35-30	52-39-09	>0.063	GD	Y	N	a
DSDP Site 177	29-58-13	25-48-27	0.063–0.5	GD	Y	N	b
Fraser River delta	42-11-47		bulk	T	N	N	c
ODP Site 888 (Nitinat Fan)	46-18-36		0.05–0.1	T	N	Y	d
ODP Site 889 (Vancouver)	41-19-40		0.05–0.1	T	N	Y	d
Bonneville reservoir	32-30-38		>0.004	T	N	N	e
Lower Columbia River	14-28-58		>0.004	T	N	N	e
Oregon-Washington shelf	16-22-62		bulk	T	N	N	f
DSDP Site 174 (Astoria Fa	36-40-24	47-23-30	0.063–0.5	GD	Y	N	g
DSDP Site 174 (abyssal)	21-27-52	69-06-25	0.063–0.5	GD	Y	N	g

* GD = Gazzi-Dickinson; T = traditional.
** Y = stained for feldspar; N = not stained.
*** Y = heavy-liquid separation; N = no separation.
a = Underwood and Hoke (2000); b = Gergen and Ingersoll (1986); c = Garrison et al. (1969); d = Chamov and Murdmaa (1994); e = Whetten et al. (1969); f = White (1970); g = Marsaglia and Ingersoll (1992).

90,000-year datum above ''reflector A'' at 1025 but below ''reflector A'' at 1024 and 1028. Echo character above ''reflector A'' also changes across the intervening basement ridge. The 0.09 Ma nannofossil datum fits shallow reflector geometries better between Sites 1026 and 1027, but the effects of channel incision and infilling render the temporal correlation of deeper reflectors more difficult (Fig. 5). These seismic-reflection data reinforce the idea that only exceptional events were large enough to spread sediment across the entire floor of the Leg 168 study area.

Sand Provenance and Dispersal

The final element of the Cascadia turbidite system to consider is the sand source. Detrital modes indicate that the sand was derived from a polymictic assemblage of igneous, metamorphic, sedimentary, and metasedimentary rocks. Our mean value for total-grain modes (Q = 35, F = 35, L = 30) plots within the generic dissected-arc field (Fig. 13) as defined by Dickinson et al. (1983). Monocrystalline data (mean of $Q_m = 46$, P = 49, and K = 5) plot within the Circum-Pacific volcano-plutonic suite of Dickinson (1982). Polycrystalline modes lie within the arc-orogen field of Dickinson and Suczek (1979), with a mean of $Q_p = 16$, $L_v = 43$, and $L_{sm} = 41$. The mean values of $L_v = 52$, $L_s = 39$, and $L_m = 9$ (Fig. 13) are consistent with a mixed magmatic-arc and rifted-continent source (Ingersoll and Suczek 1979). It is tricky, however, to expand from a generic tectonic provenance to a site-specific interpretation of source and transport route. Several watersheds need to be considered in our interpretation, and quantitative comparisons between published data are impossible because sample preparation and petrographic technique differed among investigators (Table 1). We can, in spite of this, establish some first-order constraints on dispersal path through qualitative assessments.

Regional bathymetry indicates that several overlapping pathways carried both channelized and unconfined turbidity currents into the northern part of Cascadia Basin (Fig. 1). The first path may originate as far north as Queen Charlotte Sound, where relatively small submarine canyons are incised into the western margin of Vancouver Island. Considering the location of the Leg 168 sites, and the north- to northeast-striking fabric of basement structures, south-directed transport through the Vancouver Valley and Juan de Fuca Channel systems should have functioned as the primary conduit of sandy sediment. This interpretation is supported further by the seismic-reflection expressions of north–south trending channel–levee features (Figs. 4, 5). Potential sources on the Queen Charlotte Islands and northern Vancouver Island include older volcanic, sedimentary, and granitic rocks (Muller 1977; Clague 1986), but no Quaternary volcanoes. The fresh andesitic and rhyolitic rock fragments from Leg 168 samples (Table 1) are more indicative of a mixed provenance that included neovolcanic centers. In addition, Gergen and Ingersoll (1986) demonstrated that sands from DSDP Site 177 (located north of our study area at 50° 28′ N) contain substantially higher percentages of total feldspar and more sedimentary-rock and metamorphic-rock fragments than the sands from Leg 168 sites (Fig. 13). On the basis of this comparison, we suspect that detrital sources north of Vancouver Island (i.e., Queen Charlotte Sound) did not contribute much to the sediment budget.

A second pathway for sediment to reach the study area is through Barkley, Nitinat, and Juan de Fuca canyons, all of which discharge near the apex of Nitinat Fan (Fig. 1). The confluence of Nitinat and Vancouver valleys is located just north of Sites 1026 and 1027 (Fig. 1), and the canyons connect in the upstream direction to the Strait of Juan de Fuca and the Fraser River delta (Clague et al. 1983). Geologic sources in that watershed are diverse. The Coast Plutonic Complex of western British Columbia, Washington, and northern Oregon consists mainly of granitic intrusions surrounded by sedimentary and volcanic rocks (Clague 1986). Farther east, the crystalline core of the Cascade Range exposes metamorphic–plutonic complexes, whereas the Western Cascades contain basaltic, andesitic, and dacitic lava flows intercalated with pyroclastic rocks (Blakely and Jachens 1990). Quaternary volcanoes of the High Cascades include basalt, rhyolite, and more commonly, andesite (McBirney 1978). Inboard of Vancouver Island, Garrison et al. (1969) showed that lithic grains and detrital quartz dominate the sand fraction of the Fraser River delta (Table 1). Once Fraser River sediment enters the Strait of Georgia, it mixes downstream with detritus from smaller streams that drain both southern Vancouver Island and the Olympic Peninsula (Mayers and Bennett 1973; Pharo and Barnes 1976). Common lithologies on those margins include metasedimentary rocks and marine volcanic rocks (Tabor and Cady 1978; Brandon et al. 1998). As a constraint on discharge into deeper water, Chamov and Murdmaa (1994) analyzed samples from the northern edge of Nitinat Fan (ODP Site 888) and the Vancouver slope (ODP Site 889). Compared to Leg 168 data, those average Q-F-L values are substantially depleted in total feldspar (Table 1), but this mismatch is probably an artifact of their technique. Thus, our inferred connection from source to sink falls short of being definitive.

The Columbia River (Fig. 1) provides the largest present-day point source of fluvial discharge to the southern part of Cascadia Basin, with headwaters extending eastward into the Rocky Mountains. Sedimentary strata, plus plutonic and coarse metamorphic bedrock, underlie the upper Columbia sub-basin. Flood basalt is widespread in the middle and lower basin (Beeson and Tolan 1990), and andesite from active Cascade volcanoes increases toward the river mouth. Sand trapped in Bonneville reservoir (farthest downstream dam) yields average Q-F-L values of Q = 32, F = 30, and L = 38, whereas samples between Bonneville reservoir and the river mouth are more lithic-rich (Whetten et al. 1969). Beyond the river mouth, White (1970) showed Holocene sands on the Washington–Oregon shelf to be enriched in lithic fragments relative to the Leg 168 data (Table 1). On the distal edge of Astoria Fan (DSDP Site 174), the average modes for Quaternary sands are Q = 36, F = 40, and L = 24, with roughly equal proportions of L_v and L_{sm} (Gergen and Ingersoll 1986). This petrofacies, which Marsaglia and Ingersoll (1992) attributed to mixing between

Cascade arc and Idaho batholith sources in the Columbia River watershed, comes closer than any other to matching the modal character of Leg 168 samples (Fig. 13; Table 1). The older abyssal-plain facies beneath Astoria Fan is more lithic-rich than the Quaternary (Table 1), with more abundant volcanic-rock fragments (Gergen and Ingersoll 1986). Marsaglia and Ingersoll (1992) attributed this difference in sediment composition to a shift toward more Cascade volcanic debris within the Columbia River watershed during the Pliocene. Farther south, turbidites in Escanaba Trough (a Gorda Ridge segment located south of the Blanco Fracture Zone) are likewise thought to have come from a Columbia River source (Vallier et al. 1973; Normark et al. 1994; Normark and Serra 2001). Their Q-F-L modes overlap those for Quaternary Astoria Fan, but the polycrystalline constituents contain a higher proportion of volcanic-lithic debris (Zuffa et al. 2000). Similar detrital suites have been reported from piston and gravity cores in southern Cascadia Basin (Duncan and Kulm 1970).

Our holistic assessment of bathymetry and sand composition leads us to conclude that a mixed provenance contributed sand to the northwestern part of Cascadia Basin from Vancouver Island, the Olympic Peninsula, the northern Cascades, and western British Columbia. Rock types in those watersheds are similar. Homogenization of discrete contributions during glacial erosion, plus post-glacial recycling, precludes more specific provenance fingerprints. Petrofacies are similar between Leg 168 samples and a Columbia River source, but most of the Columbia River sand has been funneled toward the southwest during lowstands through Quinault, Willapa, and Astoria canyons. It seems unlikely to us that such flows would have reached the Leg 168 transect area except during unusually large discharge events, such as the jokulhlaup outbursts that were triggered by late Wisconsinian deglaciation (Waitt 1985; Atwater 1986; Brunner et al. 1999).

CONCLUSIONS

The turbidite system of northwestern Cascadia Basin is atypical and enigmatic in many respects, because of its proximity to an active mid-ocean ridge. As in most turbidite basins, depositional character and facies architecture have been sensitive to allocyclic forcing (e.g., uplift of source terrains, glaciation, earthquakes, arc volcanism). In addition, however, the architecture of Cascadia Basin has evolved rapidly in response to intrabasinal processes, including thermal subsidence, normal faulting, ridge-related volcanism, and sedimentation. Changes to the bathymetry have forced autocyclic adjustments of individual turbidity currents and channel–levee complexes.

Intervals of recurrence have been highly variable for turbidity currents entering the Juan de Fuca ridge-flank environment; the RI values range from approximately once every 675 years to one per 27,000 years. We attribute this spatial and temporal oscillation of sediment delivery to the combined effects of inconsistent subsidence of the basement, gradual infilling of rugged basement relief, reflection and deflection of flows off bathymetric highs, intrabasinal slides and debris flows, flow stripping, channel switching and abandonment, and patchy overbank flooding.

Identification of a unique sand provenance remains elusive. Average detrital modes are Q = 35, F = 35, and L = 30; Q_m = 46, P = 49, and K = 5; L_v = 52, L_s = 39, L_m = 9; and Q_p = 15, L_v = 44, and L_{sm} = 41. With few exceptions, such values are consistent both down-hole and between the Leg 168 sites. The generic tectonic provenance for these sands is straightforward: a dissected magmatic arc blended with polymictic terranes. Watersheds displaying those geologic fingerprints are ubiquitous within the western Cordillera, so it is difficult to isolate the provenance to one specific fluvial source. The diversity and abundance of volcanic-rock fragments indicates that the source area included intermediate and silicic volcanoes of the Cascade Range.

Even if the source were unambiguous, our ability to pinpoint pathways of sediment dispersal is tempered by complications in regional bathymetry. Some of the sediment probably moved south from the western margin of Vancouver Island and Queen Charlotte Sound through Vancouver Valley and Juan de Fuca Channel (and their fossil equivalents). The main argument against a northern source is the paucity of neovolcanic centers. Detritus from an eastern source (southern Vancouver Island, Olympic Peninsula, northern Cascades, and Fraser River drainage) also entered Cascadia Basin via the Strait of Juan de Fuca. Those turbidity currents, and nepheloid-layer suspensions, flowed down Barkley, Nitinat, and Juan de Fuca canyons before spreading over the northern apex of Nitinat Fan. That pathway, we believe, has been the most active over the past 1 million years. Occasional transport from the Columbia River is also possible.

The proximity of the Juan de Fuca Ridge to the Cascadia continental margin is unusual when viewed in a global context of ocean-crust hydrothermal processes. Turbidites play a vital, though indirect, role in the ocean-crust hydrogeology. Sediment accumulates slowly above basement ridges and consists mostly of hemipelagic mud with random grain fabric. At locations where total sediment thickness remains less than ~ 50 m, we see both physical and geochemical evidence for upflow of porewater from an overpressured basement, at rates that average 2.6 mm/yr. Once burial depths reach 100–150 m, however, the grain fabric of hemipelagic mud collapses, thereby reducing seepage to rates of 0.10 mm/yr or less. Rapid influx of turbidites provides the overburden necessary to transform the physical properties of mud near the basalt–sediment contact. By accelerating the compaction process, the turbidites help impede hydrothermal exchange between fractured basaltic crust and ocean bottom water.

ACKNOWLEDGMENTS

We thank the dedicated crew, technical staff, and shipboard scientists who sailed on *JOIDES Resolution* during ODP Leg 168. B. Gomer, A. Cavin, and A. Johnston-Karas assisted in the laboratory. This research used samples provided by the Ocean Drilling Program, sponsored by the U.S. National Science Foundation and participating countries under management of Joint Oceanographic Institutions, Inc. Funding was provided by the U.S. Science Support Program grants 168-F000502, 168-F000503, and 168-F000421. Kathy Marsaglia, Colin North, and an anonymous reviewer provided helpful suggestions that improved the form and substance of the manuscript.

REFERENCES

Adams, J., 1990, Paleoseismicity of the Cascadia subduction zone: Evidence from turbidites off the Oregon–Washington margin: Tectonics, v. 9, p. 569–583.

Alexander, J., and Morris, S., 1994, Observations on experimental, nonchannelized, high-concentration turbidity currents and variations in deposits around obstacles: Journal of Sedimentary Research, v. A64, p. 899–909.

Alt, J.C., Honnorez, J., Laverne, C., and Emmermann, R., 1986, Hydrothermal alteration of a 1-km section through the upper oceanic crust, Deep Sea Drilling Project Hole 504B; mineralogy, chemistry, and evolution of seawater–basalt interactions: Journal of Geophysical Research, v. 91, p. 10,309–10,335.

Atwater, B.F., 1986, Pleistocene glacial-lake deposits of the Sanpoil River valley, northeastern Washington: U.S. Geological Survey, Bulletin 1661, 39 p.

Barnard, W.D., 1978, The Washington continental slope: Quaternary tectonics and sedimentation: Marine Geology, v. 27, p. 79–114.

Beeson, M.H., and Tolan, T.L., 1990, The Columbia River Basalt Group in the Cascade Range: A middle Miocene reference datum for structural analysis: Journal of Geophysical Research, v. 95, p. 19,547–19,559.

Blakely, R.J., and Jachens, R.C., 1990, Volcanism, isostatic residual gravity, and regional tectonic setting of the Cascade Volcanic Province: Journal of Geophysical Research, v. 95, p. 19,439–19,451.

Brandon, M.T., Roden-Tice, M.K., and Garver, J.I., 1998, Late Cenozoic exhumation of the Cascadia accretionary wedge in the Olympic Mountains, northwest Washington State: Geological Society of America, Bulletin, v. 110, p. 985–1009.

Brunner, C.A., Normark, W.R., Zuffa, G.G., and Serra, F., 1999, Deep-sea sedimentary record of the Late Wisconsin cataclysmic floods from the Columbia River: Geology, v. 27, p. 463–466.

Carlson, P.R., and Nelson, C.H., 1969, Sediments and sedimentary structures of the Astoria submarine canyon–fan system, northeast Pacific: Journal of Sedimentary Petrology, v. 39, p. 1269–1282.

Carlson, P.R., and Nelson, C.H., 1987, Marine geology and resource potential of Cascadia Basin, *in* Scholl, D.W., Grantz, A., and Vedder, J.G., eds., Geology and Resource Potential of the Continental Margin of Western North America and Adjacent Ocean Basins—Beaufort Sea to Baja California: Circum-Pacific Council for Energy and Mineral Resources, Earth Science Series, v. 6, p. 523–536.

CARSON, B., 1973, Acoustic stratigraphy, structure and history of Quaternary deposition in Cascadia Basin: Deep-Sea Research, v. 20, p. 387–396.

CARSON, B., AND MCMANUS, D.A., 1971, Analysis of turbidite correlation in Cascadia Basin, northeast Pacific Ocean: Deep-Sea Research, v. 18, p. 593–604.

CARSON, B., BAKER, E.T., HICKEY, B.M., NITTROUER, C.A., DEMASTER, D.J., THORBJARNARSON, K.W., AND SNYDER, G.W., 1986, Modern sediment dispersal and accumulation in Quinault submarine canyon—a summary: Marine Geology, v. 71, p. 1–13.

CAVIN, A., UNDERWOOD, M., FISHER, A.T., AND JOHNSTON-KARAS, A., 2000, Relations between textural characteristics and physical properties of sediments in northwestern Cascadia Basin, *in* Fisher, A.T., Davis, E.E., and Escutia, C., eds., Proceedings of the Ocean Drilling Program, Scientific Results, v. 168: College Station, Texas (Ocean Drilling Program), p. 67–84 and CD-ROM.

CHAMOV, N.P., AND MURDMAA, I.O., 1994, Coarse fraction minerals of sands in Cascadia margin sediments, *in* Carson, B., Westbrook, G.K., Musgrave, R.J., and Suess, E., eds., Proceedings of the Ocean Drilling Program, Scientific Results, v. 146: College Station, Texas (Ocean Drilling Program), p. 33–43.

CLAGUE, J.J., 1986, Bedrock geology (Canadian Cordillera), *in* Fulton, R.J., ed., Quaternary Geology of Canada and Greenland: Geological Society of America, The Geology of North America, v. K-1, p. 22–25.

CLAGUE, J.J., LUTERNAUER, J.L., AND HEBDA, R.J., 1983, Sedimentary environments and postglacial history of the Fraser Delta and lower Fraser Valley, British Columbia: Canadian Journal of Earth Sciences, v. 20, p. 1314–1326.

DAMUTH, J.E., AND EMBLEY, R.W., 1979, Upslope flow of turbidity currents on the northwest flank of the Ceara Rise: Western equatorial Atlantic: Sedimentology, v. 26, p. 825–834.

DAVIS, E.E., AND HYNDMAN, R.D., 1989, Accretion and recent deformation of sediments along the northern Cascadia subduction zone: Geological Society of America, Bulletin, v. 101, p. 1465–1480.

DAVIS, E.E., CHAPMAN, D.S., MOTTL, M.J., BENTKOWSKI, W.J., DADEY, K., FORSTER, C., HARRIS, R., NAGIHARA, S., ROHR, K., WHEAT, G., AND WHITICAR, M., 1992, FlankFlux: an experiment to study the nature of hydrothermal circulation in young oceanic crust: Canadian Journal of Earth Sciences, v. 29, p. 925–952.

DICKINSON, W.R., 1970, Interpreting detrital modes of graywacke and arkose: Journal of Sedimentary Petrology, v. 40, p. 695–707.

DICKINSON, W.R., 1982, Compositions of sandstones in circum-Pacific subduction complexes and fore-arc basins: American Association of Petroleum Geologists, Bulletin, v. 66, p. 121–137.

DICKINSON, W.R., AND SUCZEK, C.A., 1979, Plate tectonics and sandstone compositions: American Association of Petroleum Geologists, Bulletin, v. 63, p. 2164–2182.

DICKINSON, W.R., BEARD, L.S., BRAKENRIDGE, G.R., ERJAVEC, J.L., FERGUSON, R.C., INMAN, K.F., KNEPP, R.A., LINDBERG, F.A., AND RYBERG, P.T., 1983, Provenance of North American Phanerozoic sandstones in relation to tectonic setting: Geological Society of America, Bulletin, v. 94, p. 222–235.

DOLAN, J.F., BECK, C., AND OGAWA, Y., 1989, Upslope deposition of extremely distal turbidites: An example from the Tiburon Rise, west-central Atlantic: Geology, v. 17, p. 990–994.

DUKE, W.L., 1985, Hummocky cross-stratification, tropical hurricanes, and intense winter storms: Sedimentology, v. 32, p. 167–194.

DUNCAN, J.R., AND KULM, L.D., 1970, Mineralogy, provenance, and dispersal history of late Quaternary deep-sea sands in Cascadia Basin and Blanco Fracture Zone off Oregon: Journal of Sedimentary Petrology, v. 40, p. 874–877.

ELDERFIELD, H., AND SCHULTZ, A., 1996, Mid-ocean ridge hydrothermal fluxes and the chemical composition of the ocean: Annual Review of Earth and Planetary Sciences, v. 24, p. 191–224.

FISHER, A.T., 1998, Permeability within basaltic oceanic crust: Reviews of Geophysics, v. 36, p. 143–182.

FISHER, A.T., BECKER, K., AND NARASIMHAN, T.N., 1994, Off-axis hydrothermal circulation: Parametric tests of a refined model of processes at Deep Sea Drilling Project/Ocean Drilling Program site 504: Journal of Geophysical Research, v. 99, p. 3097–3121.

GARCIA, M.O., AND HULL, D.M., 1994, Turbidites from giant Hawaiian landslides: Results from Ocean Drilling Program Site 842: Geology, v. 22, p. 159–162.

GARRISON, R. E., LUTERNAUER, J.L., GRILL, E.V., MACDONALD, R.D., AND MURRAY, J.W., 1969, Early diagenetic cementation of recent sands, Fraser River delta, British Columbia: Sedimentology, v. 12, p. 27–46.

GERGEN, L.D., AND INGERSOLL, R.V., 1986, Petrology and provenance of Deep Sea Drilling Project sand and sandstone from the North Pacific Ocean and the Bering Sea: Sedimentary Geology, v. 51, p. 29–56.

GIAMBALVO, E.R., FISHER, A.T., MARTIN, J.T., DARTY, L., AND LOWELL, R.P., 2000, Origin of elevated sediment permeability in a hydrothermal seepage zone, eastern flank of the Juan de Fuca Ridge, and implications for transport of fluid and heat: Journal of Geophysical Research, v. 105, p. 913–928.

GIAMBALVO, E.R., STEEFEL, C.I., FISHER, A.T., ROSENBERG, N.D., AND WHEAT, C.G., 2002, Effect of fluid–sediment reaction on hydrothermal fluxes of major elements, eastern flank of the Juan de Fuca Ridge: Geochimica et Cosmochimica Acta, v. 66, p. 1739–1757.

GRIGGS, G.B., AND KULM, L.D., 1970, Sedimentation in Cascadia deep-sea channel: Geological Society of America, Bulletin, v. 81, p. 1361–1384.

HAMPTON, M.A., KARL, H.A., AND KENYON, N.H., 1989, Sea-floor drainage features of Cascadia Basin and the adjacent continental slope, northeast Pacific Ocean: Marine Geology, v. 87, p. 249–272.

HERZER, R.H., 1978, Submarine canyons and slumps on the continental slope off southern Vancouver Island: Geological Survey of Canada, Current Research, v. 78–1A, p. 357–360.

HISCOTT, R.N., COLELLA, A., PEZARD, P., LOVELL, M.A., AND MALINVERNO, A., 1992, Sedimentology of deep-water volcaniclastics, Oligocene Izu–Bonin forearc basin, based on Formation Micro-Scanner images, *in* Taylor, B., Fujioka, K., et al., Proceedings of the Ocean Drilling Program, Scientific Results, v. 126: College Station, Texas (Ocean Drilling Program), p. 467–486.

HOUGHTON, H.F., 1980, Refined techniques for staining plagioclase and alkali feldspars in thin section: Journal of Sedimentary Petrology, v. 50, p. 629–931.

INGERSOLL, R.V., AND SUCZEK, C.A., 1979, Petrology and provenance of Neogene sand from Nicobar and Bengal fans, DSDP Sites 211 and 218: Journal of Sedimentary Petrology, v. 49, p. 1217–1228.

INGERSOLL, R.V., BULLARD, T.F., FORD, R.L., GRIMM, J.P., PICKLE, J.D., AND SARES, S.W., 1984, The effect of grain size on detrital modes: a test of the Gazzi–Dickinson point-counting method: Journal of Sedimentary Petrology, v. 54, p. 103–116.

JACOBSON, R.S., 1992, Impact of crustal evolution on changes of the seismic properties of the uppermost ocean crust: Reviews of Geophysics, v. 30, p. 23–42.

JONES, K.P.N., MCCAVE, I.N., AND PATEL, P.D., 1988, A computer-interfaced SediGraph for modal size analysis of fine-grained sediment: Sedimentology, v. 35, p. 163–172.

KARL, H.A., HAMPTON, M.A., AND KENYON, N.H., 1989, Lateral migration of Cascadia Channel in response to accretionary tectonics: Geology, v. 17, p. 144–147.

KARATO, S., AND BECKER, K., 1983, Porosity and hydraulic properties of sediments from the Galapagos spreading center and their relationship to hydrothermal circulation in the oceanic crust: Journal of Geophysical Research, v. 88, p. 1009–1017.

KELTS, K., AND ARTHUR, M.A., 1981, Turbidites after ten years of deep-sea drilling—wringing out the mop?, *in* Warme, J.E., Douglas, R.C., and Winterer, E.L., eds., The Deep Sea Drilling Project: A Decade of Progress: SEPM, Special Publication 32, p. 91–127.

KNELLER, B., AND BUCKEE, C., 2000, The structure and fluid mechanics of turbidity currents: a review of some recent studies and their geological implications: Sedimentology, v. 47, p. 62–94.

KNELLER, B., AND MCCAFFREY, W., 1999, Depositional effects of flow nonuniformity and stratification within turbidity currents approaching a bounding slope: deflection, reflection, and facies variation: Journal of Sedimentary Research, v. 69, p. 980–991.

KNELLER, B., EDWARDS, D., MCCAFFREY, W., AND MOORE, R., 1991, Oblique reflection of turbidity currents: Geology, v. 14, p. 250–252.

KULM, L.D., AND FOWLER, G.A., 1974, Oregon continental margin structure and stratigraphy: a test of the imbricate thrust model, *in* Burk, C.A., and Drake, C.L., eds., The Geology of Continental Margins: New York, Springer-Verlag, p. 261–284.

MACKAY, M.E., 1995, Structural variation and landward vergence at the toe of the Oregon accretionary prism: Tectonics, v. 14, p. 1309–1320.

MARSAGLIA, K.M., AND INGERSOLL, R.V., 1992, Compositional trends in arc-related, deep-marine sand and sandstone: a reassessment of magmatic-arc provenance: Geological Society of America, Bulletin, v. 104, p. 1637–1649.

MAYERS, I.R., AND BENNETT, L.C., 1973, Geology of the Strait of Juan de Fuca: Marine Geology, v. 15, p. 89–117.

MCBIRNEY, A.R., 1978, Volcanic evolution of the Cascade Range: Annual Review of Earth and Planetary Sciences, v. 6, p. 437–456.

MOTTL, M.J., AND WHEAT, C.G., 1994, Hydrothermal circulation through mid-ocean ridge flanks: fluxes of heat and magnesium: Geochimica et Cosmochimica Acta, v. 58, p. 2225–2237.

MOTTL, M.J., WHEAT, C.G., BAKER, E., BECKER, N., DAVID, E., FEELY, R., GREHAN, A., KADKO, D., LILLEY, M., MASSOTH, G., MOYER, C., AND SANSONE, F., 1998, Warm springs discovered on 3.5 Ma oceanic crust, eastern flank of the Juan de Fuca Ridge: Geology, v. 26, p. 51–54.

MUCK, M.T., AND UNDERWOOD, M.B., 1990, Upslope flow of turbidity currents: a comparison among field observations, theory, and laboratory models: Geology, v. 18, p. 54–57.

MULDER, T., AND SYVITSKI, J.P.M., 1995, Turbidity currents generated at river mouths during exceptional discharges to the world ocean: Journal of Geology, v. 103, p. 285–299.

MULLER, J.E., 1977, Evolution of the Pacific Margin, Vancouver Island, and adjacent regions: Canadian Journal of Earth Sciences, v. 14, p. 2062–2085.

MUTTI, E., AND NORMARK, W.R., 1987, Comparing examples of modern and ancient turbidite systems: problems and concepts, *in* Leggett, J.K., and Zuffa, G.G., eds., Marine Clastic Sedimentology: Boston, Graham & Trotman, p. 1–38.

NELSON, C.H., 1976, Late Pleistocene and Holocene depositional trends, processes and history of Astoria deep-sea fan, northeast Pacific: Marine Geology, v. 20, p. 129–173.

NELSON, C.H., 1982, Modern shallow-water graded sand layers from storm surges, Bering Shelf: a mimic of Bouma sequences and turbidite systems: Journal of Sedimentary Petrology, v. 52, p. 537–546.

NELSON, C.H., CARLSON, P.R., BYRNE, J.V., AND ALPHA, T.R., 1970, Development of the Astoria canyon–fan physiography and comparison with similar systems: Marine Geology, v. 8, p. 259–291.

NORMARK, W.R., AND SERRA, F., 2001, Vertical tectonics in northern Escanaba Trough as recorded by thick late Quaternary turbidites: Journal of Geophysical Research, v. 106, p. 13,793–13,802.

NORMARK, W.R., GUTMACHER, C.E., ZIERENBERG, R.A., WONG, F.L., AND ROSENBAUER, R.J., 1994, Sediment fill of Escanaba Trough, *in* Morton, J.L., Zierenberg, R.A., and Reiss, C.A., eds., Geologic, Hydrothermal, and Biologic Studies at Escanaba Trough, Gorda Ridge, Offshore Northern California: U.S. Geological Survey, Bulletin 2002, p. 91–128.

PANTIN, H.M., AND LEEDER, M.R., 1987, Reverse flow in turbidity currents: the role of internal solitons: Sedimentology, v. 34, p. 1143–1155.

PEARCE, T.J., AND JARVIS, I., 1992, Composition and provenance of turbidite sands: late Quaternary, Madeira Abyssal Plain: Marine Geology, v. 109, p. 21–51.

PHARO, C.H., AND BARNES, W.C., 1976, Distribution of surficial sediments of the central and southern Strait of Georgia, British Columbia: Canadian Journal of Earth Sciences, v. 13, p. 684–696.

PICKERING, K.T., UNDERWOOD, M.B., AND TAIRA, A., 1992, Open-ocean to trench turbidity-current flow in the Nankai Trough: flow collapse and reflection: Geology, v. 20, p. 1099–1102.

Pilkey, O.H., Locker, S.D., and Cleary, W.J., 1980, Comparison of sand-layer geometry on flat floors of 10 modern depositional basins: American Association of Petroleum Geologists, Bulletin, v. 64, p. 841–856.

Piper, D.J.W., and Normark, W.R., 1983, Turbidite depositional patterns and flow characteristics, Navy submarine fan, California Borderland: Sedimentology, v. 30, p. 681–694.

Saettler, K.D., 1998, Composition, provenance, and depositional patterns of turbidites and hemipelagic muds, northwestern Cascadia Basin [unpublished M.S. thesis]: Columbia, University of Missouri, 212 p.

Sclater, J.G., Crowe, J., and Anderson, R.N., 1976, On the reliability of oceanic heat flow averages: Journal of Geophysical Research, v. 81, p. 2997–3006.

Sclater, J.G., Jaupart, C., and Galson, D., 1980, Heat flow through oceanic and continental crust and the heat loss of the Earth: Reviews of Geophysics, v. 18, p. 269–311.

Shipboard Scientific Party, 1973, Site 174, *in* Kulm, L.D., von Huene, R., et al., Initial Reports of the Deep Sea Drilling Project, Volume 18: Washington, D.C., U.S. Government Printing Office, p. 97–167.

Shipboard Scientific Party, 1994, Site 888, *in* Westbrook, G.K., Carson, B., Musgrave, R.J., et al., Proceedings of the Ocean Drilling Program, Initial Reports, Volume 146: College Station, Texas (Ocean Drilling Program), p. 55–125.

Shipboard Scientific Party, 1997a, Introduction and summary: hydrothermal circulation and its consequences on the eastern flank of the Juan de Fuca Ridge, *in* Davis, E.E., Fisher, A.T., Firth, J.V., et al., Proceedings of the Ocean Drilling Program, Initial Reports, v. 168: College Station, Texas (Ocean Drilling Program), p. 7–21.

Shipboard Scientific Party, 1997b, Hydrothermal transition transect (Sites 1023, 1024, and 1025), *in* Davis, E.E., Fisher, A.T., Firth, J.V., et al., Proceedings of the Ocean Drilling Program, Initial Reports, v. 168: College Station, Texas (Ocean Drilling Program), p. 49–100.

Shipboard Scientific Party, 1997c, Rough basement transect (Sites 1026 and 1027), *in* Davis, E.E., Fisher, A.T., Firth, J.V., et al., Proceedings of the Ocean Drilling Program, Initial Reports, v. 168: College Station, Texas (Ocean Drilling Program), p. 101–160.

Shipboard Scientific Party, 1997d, Buried basement transect (Sites 1028, 1029, 1030, 1031, and 1032), *in* Davis, E.E., Fisher, A.T., Firth, J.V., et al., Proceedings of the Ocean Drilling Program, Initial Reports, v. 168: College Station, Texas (Ocean Drilling Program), p. 161–212.

Singer, J.K., Anderson, J.B., Ledbetter, M.T., McCave, I.N., Jones, K.P.N., and Wright, R., 1988, An assessment of analytical techniques for the size analysis of fine-grained sediments: Journal of Sedimentary Petrology, v. 58, p. 534–543.

Snelgrove, S.H., and Forster, C.B., 1996, Impact of seafloor sediment permeability and thickness on off-axis hydrothermal circulation: Juan de Fuca Ridge eastern flank: Journal of Geophysical Research, v. 101, p. 2915–2925.

Spinelli, G.A., Zuehlsdorff, L., Fisher, A.T., Wheat, C.G., Mottl, M., Spiess, V., and Giambalvo, E.R., 2004, Hydrothermal seepage patterns above a buried basement ridge, eastern flank of the Juan de Fuca Ridge: Journal of Geophysical Research, v. 109, B01102, doi: 10.1029/2003JB002476.

Stein, R., 1985, Rapid grain-size analyses of clay and silt fraction by Sedigraph 5000D: comparison with Coulter Counter and Atterberg methods: Journal of Sedimentary Petrology, v. 55, p. 590–615.

Stein, C.A., and Stein, S., 1994, Comparison of plate and asthenospheric flow models for the thermal evolution of oceanic lithosphere: Geophysical Research Letters, v. 21, p. 709–712.

Stokke, P.R., Carson, B., and Baker, E.T., 1977, Comparison of the bottom nepheloid layer and late Holocene deposition on Nitinat Fan: implications for lutite dispersal and deposition: Geological Society of America, Bulletin, v. 88, p. 1586–1592.

Su, X., Baumann, K.-H., and Thiede, J., 2000, Calcareous nannofossils from Leg 168: biochronology and diagenesis, *in* Fisher, A.T., Davis, E.E., and Escutia, C., eds., Proceedings of the Ocean Drilling Program, Scientific Results, v. 168: College Station, Texas (Ocean Drilling Program), p. 39–50.

Tabor, R.W., and Cady, W.H., 1978, The structure of the Olympic Mountains, Washington—analysis of a subduction zone: U.S. Geological Survey, Professional Paper 1033, p. 1–38.

Underwood, M.B., 2002, Strike-parallel variations in clay minerals and fault vergence in the Cascadia subduction zone: Geology, v. 30, p. 155–158.

Underwood, M.B., and Hoke, K.M., 2000, Composition and provenance of turbidite sand and hemipelagic mud in northwestern Cascadia Basin, Leg 168 of the Ocean Drilling Program, *in* Fisher, A.T., Davis, E.E., and Escutia, C., eds., Proceedings of the Ocean Drilling Program, Scientific Results, v. 168: College Station, Texas (Ocean Drilling Program), p. 51–65 and CD-ROM.

Vallier, T.L., Harold, P.J., and Gerdley, W.A., 1973, Provenance and dispersal patterns of turbidite sand in Escanaba Trough, northeastern Pacific Ocean: Marine Geology, v. 15, p. 67–87.

Waitt, R.B., 1985, Case for periodic, colossal jokulhlaups from Pleistocene glacial Lake Missoula: Geological Society of America, Bulletin, v. 96, p. 1271–1286.

Weaver, P.P.E., Rothwell, R.G., Ebbing, J., Gunn, D., and Hunter, P.M., 1992, Correlation, frequency of emplacement and source directions of megaturbidites on the Madeira Abyssal Plain: Marine Geology, v. 109, p. 1–20.

Wheat, C.G., and Mottl, M.J., 1994, Hydrothermal circulation, Juan de Fuca Ridge eastern flank: factors controlling basement water composition: Journal of Geophysical Research, v. 99, p. 3067–3080.

Whetten, J.T., Kelly, J.C., and Hanson, L.G., 1969, Characteristics of Columbia River sediment and sediment transport: Journal of Sedimentary Petrology, v. 39, p.1149–1166.

White, S.M., 1970, Mineralogy and geochemistry of continental shelf sediments off the Washington–Oregon coast: Journal of Sedimentary Petrology, v. 40, p. 38–54.

Zdanowicz, C.M., Zielinski, G.A., and Germani, M.S. 1999, Mount Mazama eruption: Calendrical age verified and atmospheric impact assessed: Geology, v. 27, p. 621–624.

Zierenberg, R.A., and Miller, D.J., 2000, Overview of Ocean Drilling Program Leg 169: Sedimented Ridges II: Proceedings of the Ocean Drilling Program, Scientific Results, v. 169: College Station, Texas (Ocean Drilling Program), p. 1–39.

Zuffa, G.G., Normark, W.R., Serra, F., and Brunner, C.A., 2000, Turbidite megabeds in an oceanic rift valley recording jokulhlaups of late Pleistocene glacial lakes of the western United States: Journal of Geology, v. 108, p. 253–274.

Zühlsdorff, L., and Spiess, V., 2001, Modeling seismic reflection patterns from Ocean Drilling Program Leg 168 core density logs: insight into lateral variations in physical properties and sediment input at the eastern flank of the Juan de Fuca Ridge: Journal of Geophysical Research, v. 106, p. 16,119–16,133.

Zühlsdorff, L., and Spiess, V., in press, Sedimentation patterns, forced folding and fluid upflow above a buried basement ridge—results from a high resolution 3D survey at the eastern Juan de Fuca Ridge: Journal of Geophysical Research.

Zühlsdorff, L., Spiess, V., Hübscher, C., and Breitzke, M., 1999, Seismic reflectivity anomalies in sediments at the eastern flank of the Juan de Fuca Ridge: evidence for fluid migration?: Journal of Geophysical Research, v. 104, p. 15351–15364.

Received 25 July 2002; accepted 30 June 2004.